Neurobiology of Disease 165 (2022) 105632

Contents lists available at ScienceDirect

Neurobiology of Disease

journal homepage: www.elsevier.com/locate/ynbdi

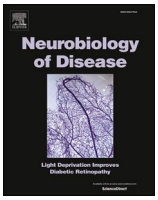

TNAP upregulation is a critical factor in Tauopathies and its blockade ameliorates neurotoxicity and increases life-expectancy

Álvaro Sebastián-Serrano [a,b], Jesús Merchán-Rubira [c], Caterina Di Lauro [a,b], Carolina Bianchi [a,b], Lucía Soria-Tobar [a], Sonoko Narisawa [e], José L. Millán [e], Jesús Ávila [c,d], Félix Hernández [c,d,1,*], Miguel Díaz-Hernández [a,b,**,2]

[a] Department of Biochemistry and Molecular Biology, Veterinary School, Complutense University of Madrid, Avda. Puerta de Hierro S/N, 28040 Madrid, Spain
[b] Instituto de Investigación Sanitaria del Hospital Clínico San Carlos, IdISSC, Madrid, Spain
[c] Centro de Biología Molecular Severo Ochoa (CSIC-UAM), Universidad Autónoma de Madrid, C/ Nicolás Cabrera, 1, 28049 Madrid, Spain
[d] Centro de Investigación Biomédica en Red sobre Enfermedades Neurodegenerativas (CIBERNED), C/ Valderrebollo, 528031 Madrid, Spain
[e] Sanford Burnham Prebys Medical Discovery Institute, La Jolla, CA, USA

ARTICLE INFO

Keywords:
Muscarinic receptor M1
Neuronal death
Tau spreading
Levamisole
PS19

ABSTRACT

Tauopathies are a family of neurodegenerative diseases characterized by the presence of abnormally hyperphosphorylated Tau protein. Several studies have proposed that increased extracellular Tau (eTau) leads to the spread of cerebral tauopathy. However, the molecular mechanisms underlying eTau-induced neurotoxicity remain unclear. Previous in vitro studies reported that the ecto-enzyme tissue-nonspecific alkaline phosphatase (TNAP) dephosphorylate eTau at different sites increasing its neurotoxicity. Here, we confirm TNAP protein upregulation in the brains of Alzheimer's patients and found a similar TNAP increase in Pick's disease patients and P301S mice, a well-characterized mouse model of tauopathies. Interestingly, the conditional overexpression of TNAP causes intracellular Tau hyperphosphorylation and aggregation in cells neighbouring those overexpressing the ectoenzyme. Conversely, the genetic disruption of TNAP reduced the dephosphorylation of eTau and decreased neuronal hyperactivity, brain atrophy, and hippocampal neuronal death in P301S mice. TNAP haploinsufficiency in P301S mice prevents the decreased anxiety-like behaviour, motor deficiency, and increased memory capacity and life expectancy. Similar results were observed by the in vivo pharmacological blunting of TNAP activity. This study provides the first in vivo evidence demonstrating that raised TNAP activity is critical for Tau-induced neurotoxicity and suggest that TNAP blockade may be a novel and efficient therapy to treat tauopathies.

1. Introduction

Tauopathies are a set of neurodegenerative disorders characterized by the presence of aberrant intracellular aggregates that are assembled by hyperphosphorylated Tau protein. Tauopathies include Alzheimer's disease (AD), Pick's disease (PiD), argyrophilic grain disease, progressive supranuclear palsy, corticobasal degeneration, and frontotemporal dementia with parkinsonism (Lee et al., 2001). In AD, Tau pathology propagates following a well-defined anatomical pattern, starting in the brainstem and progressing towards the entorhinal cortex, goes into

Abbreviations: CSF, cerebrospinal fluid; DAB, 3,3′-diaminobenzidine; EPM, elevated-plus maze test; eTau, extracellular Tau protein; M1R, muscarinic receptors M1; OF, open field test; qRT-PCR, Quantitative Real-Time PCR; TNAP, tissue-nonspecific alkaline phosphatase; TNAP OE, TNAP conditional overexpression; WT, Wild-type; i.c.v, intracerebroventricular; LPS, lipopolysaccharide; AD, Alzheimer's disease; PiD, Pick's disease; Thio-T, Thioflavin-T.

* Correspondence to Félix Hernández, Centro de Biología Molecular Severo Ochoa (CSIC-UAM), Universidad Autónoma de Madrid, C/ Nicolás Cabrera, 1. 28049 Madrid, Spain.

** Correspondence to Miguel Díaz-Hernández, Department of Biochemistry and Molecular Biology, Veterinary School, Complutense University of Madrid, Avda. Puerta de Hierro S/N, 28040 Madrid, Spain.

E-mail addresses: fhernandez@cbm.csic.es (F. Hernández), migueldiaz@ucm.es (M. Díaz-Hernández).

[1] Postal address: CBMSO (CSIC-UAM), C/ Nicolás Cabrera, 1. 28,049 Madrid, Spain.

[2] Postal address: Dpto. Bioquímica y Biología Molecular, Facultad de Veterinaria, Universidad Complutense de Madrid, Avenida Puerta de Hierro s/n, 28,040 Madrid Spain.

https://doi.org/10.1016/j.nbd.2022.105632
Received 19 July 2021; Received in revised form 11 January 2022; Accepted 12 January 2022
Available online 19 January 2022

neocortical association areas, and reaching primary fields of the neocortex (Braak and Del Tredici, 2011). The progression of this disease correlates with neuronal loss and cognitive decline of the patient (Bondareff et al., 1989; Lee et al., 2001). A recently gathered body of evidence suggests that extracellular Tau protein (eTau) is the main agent that causes the interneuronal propagation of neurofibrillary lesions and thus drives the spread of Tau toxicity throughout the brain (Wang and Mandelkow, 2016). In this regard, intracranial injection of different forms of Tau protein, such as fibrils (Clavaguera et al., 2009; Peeraer et al., 2015), filaments (Ahmed et al., 2014), oligomers (Levarska et al., 2013) or monomers (Michel et al., 2014), leads to the spread of pathological Tau from the injected site to anatomically connected regions of the brain. In support of these observations, elevated eTau levels have been reported in cerebrospinal fluid (CSF) samples from AD patients (Kurz et al., 1998). Consequently, it was postulated that the down-regulation of eTau levels by immunotherapeutic approaches may provide a new strategy to halt Tau propagation (Sebastian-Serrano et al., 2018a). However, active immunotherapy seeks to stimulate the patient's immune system reported harmful effects (Rosenmann et al., 2006; Rozenstein-Tsalkovich et al., 2013), and passive immunotherapy through the administration of selective antibodies against Tau, although reduced Tau-induced pathology, failed to increase the life expectancy in tauopathy mouse models (d'Abramo et al., 2013; Wisniewski and Goni, 2015). Moreover, the fact that the molecular mechanisms involved in the pathological spread of eTau remain unknown has recently led to question whether the spread of Tau and Tau-induced neurotoxicity are closely coupled (Chang et al., 2021). Therefore, further studies are required to elucidate the neurotoxic mechanisms associated with eTau as well those leading to progressive Tau phosphorylation with the aim of opening new therapeutic windows for the treatment of tauopathies.

Previous studies have noted that the ecto-enzyme tissue-nonspecific alkaline phosphatase (TNAP) plays a key role in the neurotoxic effect induced by eTau (Diaz-Hernandez et al., 2010; Gomez-Ramos et al., 2006; Gomez-Ramos et al., 2009; Gomez-Ramos et al., 2008). Using in vitro approaches, earlier works reported that TNAP dephosphorylates hyperphosphorylated eTau at different sites (Diaz-Hernandez et al., 2010). In cultured hippocampal neurons, specific activation of M1 and M3 muscarinic receptors by TNAP-dephosphorylated eTau impairs intracellular calcium homeostasis, thereby inducing cell death (Gomez-Ramos et al., 2009; Gomez-Ramos et al., 2008). Consistent with the involvement of TNAP in Tau pathology, higher cerebral and plasmatic TNAP activity was detected both in sporadic and familial AD patients compared with the corresponding age-matched controls, and it was inversely correlated with cognitive function (Vardy et al., 2012). On the contrary, a partial dephosphorylation of the injected Tau was also reported to decrease its own spreading (Hu et al., 2016). To clarify this issue, here we examined whether TNAP is an essential factor in Tau pathology. Accordingly, increased TNAP protein and messenger levels were detected in hippocampal necropsies from patients with distinct tauopathies. Brain samples from a well-characterized tauopathy mouse model (P301S, also known as the PS19 line) (Yoshiyama et al., 2007) showed a similar rise in TNAP levels and activity, which impacts on the phosphorylation rate of eTau at specific sites. We assess the potential role of TNAP as a trigger for Tau pathology using a conditional transgenic mouse model to induce TNAP overexpression. In addition, we evaluated if the genetic or pharmacological inactivation of TNAP in P301S mice is a potential therapeutic approach to slow down or halt the progression of the disease. Based on these observations, selective blood-brain barrier-permeable TNAP antagonist drugs emerge as a novel and promising therapeutic strategy for these diseases.

2. Material and methods

2.1. Human brain tissue samples

Human samples were provided by the *Banco de Tejidos Fundación Cien* (BT-CIEN, Madrid, Spain). Table 1 summarizes the gender and age of the patients with AD and PiD from whom the hippocampal post-mortem samples were collected (Table 1). All AD and PiD cases included in this study met these diseases' clinical and neuropathological diagnostic criteria.

2.2. Animals

All animal procedures were carried out at the Universidad Complutense de Madrid, in compliance with National and European regulations (RD1201/2005; 86/609/CEE) and following the guidelines of the International Council for the Laboratory Animal Science. All surgeries were performed under isoflurane (1-chloro-2, 2, 2-trifuoroethyl-difluormethylether) anaesthesia (Isovet®, BRAUN, Rubi, Barcelona, Spain), and all efforts were made to minimize suffering.

TNAP null mice were generated by the inactivation of the mouse *Akp2* gene, as previously described (Narisawa et al., 1997). $Hprt^{ALPL}$ knock-in mice (TNAP OE) were generated by GenOway (Lyon, France) using their proprietary "Quick Knock-in™" technology, as previously described (Sheen et al., 2015). The P301S mice were obtained from The Jackson Laboratory: line B6; C3-Tg (Prnp-MAPT*P301S)PS19Vle/J; stock number 008169. The original B6C3H/F1 genetic background was changed to C57BL/6 J by back-crossing them with C57 animals in our laboratory. Double P301S;$TNAP^{+/-}$ animals were generated by crossing heterozygote $P301S^{+/-}$ and heterozygote $TNAP^{+/-}$ mice. All mice were housed with food and water available ad libitum and maintained in a temperature-controlled environment on a 12/12 h light/dark cycle with light onset at 08:00 a.m. Investigators were blinded to the group allocation during the animal experiments.

We used 40 wild-type (WT) mice, 18 females and 22 males; 34 $P301S^{+/-}$ mice, 17 females, and 17 males; 14 $TNAP^{+/-}$, 8 females and 6 males; 18 $P301S^{+/-}$; $TNAP^{+/-}$ mice, 9 females, and 9 males; 5 TNAP OE mice, 2 females and 3 males. When the animals were divided into the different groups for whatever procedure, we kept the gender variable balanced among all groups.

2.3. TNAP antagonist and LPS treatment

Based on previous work studying the levamisole bioavailability after oral or intramuscular administration (Fernandez et al., 1998), this blood-brain barrier permeable TNAP inhibitor (Lin and Tsai, 2006) was diluted at 23 mg/mL in vehicle solution. Vehicle solution was calcium-

Table 1
Case information for Control, Alzheimer's and Pick's disease and cases.

Diagnosis	Gender	Age (years)	Post-mortem delay (hours)
Alzheimer	M	76	8
Alzheimer	M	68	7
Alzheimer	F	65	5
Alzheimer	M	57	7
Alzheimer	M	91	6
Alzheimer	F	86	7
Alzheimer	F	94	9
Alzheimer	M	63	6
Alzheimer	M	81	4
Alzheimer	F	66	7
Alzheimer	F	70	8
Pick	F	86	8
Pick	M	77	4
Pick	F	89	4
Pick	M	70	7
Pick	F	79	6
Control	F	61	8
Control	F	58	5
Control	F	83	4
Control	F	74	7
Control	M	86	5

M, male. F, female. All samples are hippocampus.

and magnesium-free PBS (137 mM NaCl, 2.7 mM KCl, 5 mM Na_2HPO_4 $7H_2O$, 1.4 mM KH_2PO_4; pH 7.4) plus 0.2% DMSO. 12.5 μL of levamisole corresponding to a dosage of 9.58 mg per Kg of body weight or the same volume of vehicle solution were daily intraperitoneally injected to 9-months-old P301S and WT mice per two weeks. The treatment protocol followed a single-blind design, by which the experimenter was unaware of the genotype and treatment applied to each mouse (n = 6–5 mice per group and condition). After treatment, mice were sacrificed, and brain tissue was processed to perform immunoblot and immunohistochemical analyses. TNAP activity on brain slices was measured to evaluate the capacity of levamisole to block the cerebral activity of this enzyme.

The second TNAP inhibitor SBI-425 was intracerebroventricular (i.c.v) administered as previously reported (Sebastian-Serrano et al., 2016). Briefly, 6-month-old mice were anesthetized with isoflurane diluted in 50% O_2. The scalp was incised along the midline, and one hole was made at the appropriate stereotaxic coordinates from Bregma (mediolateral, 0.95 mm; anteroposterior, 0.4 mm; dorsoventral, 2.5 mm). 2 μL of 60 mM SBI-425 or vehicle solution were i.c.v. infused at a rate of ≈1 μL/min (n = 4–3 mice per group and condition). After 24 h CSF samples were collected.

To elucidate whether neuroinflammation might cause upregulated TNAP expression, we induced an acute-neuroinflammation to 6 to 9-month-old WT mice by intraperitoneal administration of lipopolysaccharide (LPS) as previously reported (Garcia et al., 2018). Briefly, mice were intraperitoneally treated with either sterile PBS or LPS (5 mg/kg, *Escherichia coli*, serotype 055: B5; Millipore Sigma) and sacrificed 24 h after injection.

2.4. Behavioural studies

All the animals were handled for at least 3–4 consecutive days before testing. They were randomly tested, and experimenters were blinded to the genotype of mice during the animal experiments. All mice were studied by means of behavioural tests at 7- and 9-months-old.

2.5. Elevated plus maze

The elevated plus-maze consisted of two open arms (50 × 10 cm) and two closed arms of the same size with opaque walls. The arms and central square were made of white plastic plates and placed 50 cm above the floor. Arms of the same type were arranged at opposite sides to each other. Each mouse was placed in the central square of the maze, facing one of the closed arms. Mouse behaviour was recorded during a 5-min test period. The whole apparatus was carefully cleaned with alcohol (70° proof) after each use. The number of entries into and the time spent in open and closed arms were recorded. The illumination level was around 150 lx at the center of the maze. For data analysis, we used the following measure: time in open arms versus time in open and closed arms. Data acquisition and analysis were performed automatically using Any-Maze software (Stoelting Co, Wood Dale, IL, USA).

2.6. Open field

The open field test is a behavioural motor task aimed to determine the general locomotor activity of experimental animals, their willingness to explore new environments and their anxiety levels. Mice were placed in the center of a translucent methacrylate box measuring 45 × 45 × 40 cm and recorded for 10 min. Animal movements in the box were quantified using Any-maze software (Stoelting Co, Wood Dale, IL, USA). The computer program also allowed us to discriminate when the animal was located in the center (17 × 17 cm) or at the periphery (the surrounding area) of the arena. The apparatus was located in a sound-proof room, and the experimental area was homogeneously illuminated at about 70 lx. The whole apparatus was carefully cleaned with alcohol (70° proof) after each use. Total number of entries to the center was represented, and the total distance travelled.

2.7. Novel object location

This test exploits the inherent preference of mice for novelty in order to reveal memory of previously encountered objects. In this regard, it evaluates spatial learning, which relies heavily on hippocampal activity. Mice were habituated to the open testing box during the open field test (10 min). During the memory acquisition trial, each mouse was allowed to explore two identical objects for 10 min. For the memory retention phase, animals were exposed for 10 min to the same objects, but one of them was moved to a new location. Object exploration time was recorded when the mouse touched the object directly with its nose, mouth or forepaws. The discrimination index was calculated as the time spent near the new object divided by the cumulative time spent with both objects. Results are expressed as recognition index.

2.8. Rotarod test

The rotarod test is a behavioural task that assesses motor coordination. In this study, we used an accelerating rotarod apparatus (Ugo Basile, Varese, Italy). After a training period of two days (first day: 4 rpm for 1 min, 4 repetitions; second day: 4–8 rpm for 2 min, 4 repetitions), on the third day the rotarod was accelerated from 4 to 40 rpm over 5 min, also with four repetitions. Mean latency to fall was calculated. In the second round, only one day of training was required before the test.

2.9. Stereotaxic injection of lentivirus

To increase the hippocampal TNAP expression, six-month-old TNAP OE or WT mice (n = 5 per genotype) were randomly anesthetized with isoflurane diluted in 50% O_2 and the experimenter was blinded to the genotype of mice during injection procedure. The scalp was incised along the midline and the skull drilled before 2 μL solution containing pLOX-CW-CRE lentivirus (Lim et al., 2010) was injected into the right hippocampus (mediolateral, 1 mm; anteroposterior, 2 mm; dorsoventral, 1.8 mm relative to the bregma) using a Hamilton syringe at a rate of ≈0.5 μL/min. After the injection, we let the needle rest in place for 5 min to prevent regurgitation of the virus during removal. pLOX-CW-CRE lentivirus was kindly gifted by professors Alfredo Gimenez-Cassina and Javier Díaz-Nido (Centro de Biología Molecular "Severo Ochoa" and Universidad Autónoma de Madrid respectively. Madrid, Spain).

2.10. Tissue processing for immunohistochemistry and immunofluorescence

Mice were anesthetized using a mix of ketamine (80–200 mg/kg) and xylazine (7–20 mg/kg) diluted in PBS, administered as a single intraperitoneal injection. They were perfused transcardially with PBS followed by cold PFA (pH 7.4) (Sigma-Aldrich). Brains were dissected immediately and placed overnight in 4% PFA at 4 °C for post-fixation. Excess PFA was removed with three washes in PBS. Next, the fixed brains were placed in 30% sucrose in PBS overnight at 4 °C for cryoprotection. Samples were then embedded in OCT compound (Sakura, Finetek, Torrance, CA) and frozen using dry ice. Finally, 25-μm floating sections were cut in parasagittal or coronal planes with a cryostat (CM1950, Leica Microsystems) and stored in a solution of 30% ethylene glycol, 30% glycerol and 0.1 M PBS at −20 °C until processed.

2.11. Immunohistochemistry and immunofluorescence

For immunohistochemical analysis, mouse sections were pre-treated for 45 min with 1% H_2O_2 in PBS to inactivate endogenous peroxidase. Afterwards, sections were washed in PBS, blocked for 1 h. in block solution (1% bovine serum albumin (BSA), Sigma-Aldrich, 5% fetal bovine serum (FBS), and 0.2% Triton X-100, Sigma-Aldrich, in PBS) and finally

incubated ON at 4 °C with rabbit anti- muscarinic receptor M1 (M1R, catalog AB5164, Merck Millipore 1:250), rabbit anti-TNAP (1:500) and rabbit anti-cleave caspase-3 (catalog 9661, Cell Signaling, 1:50). Subsequently, brain sections were washed with PBS buffer and incubated for 1 h with biotinylated antibodies. After being washed twice with PBS, sections were incubated with avidin-biotin complex using the Elite Vectastain kit (Vector Laboratories, Burlingame, CA, USA) and chromogen reactions were performed with diaminobenzidine (DAB; Sigma-Aldrich) and 0.003% H_2O_2 for 10 min. Once washed with distilled water, sections were mounted on glass slides and dried, after which they were coverslipped using FluorSave (Calbiochem).

For immunofluorescence studies, mouse slices were boiled in citrate buffer, washed in PBS, blocked for 1 h at room temperature (RT) with 5% FBS and 1% BSA (Sigma-Aldrich) in PBS containing 0.2% Triton X-100 (blocking solution) and then incubated at 37 °C for 1 h or overnight at 4 °C with primary antibodies diluted as follows: mouse anti-NeuN (catalog MAB377, Millipore, 1:500), rabbit anti-NeuN (catalog ABN78, Merck, 1:1000), rabbit anti-Calbindin (catalog CB-38, Swant, 1:1000) rabbit anti-TNAP (catalog GTX100817, Gentex, 1:500), mouse anti-Tau AT8 (phospho Tau, Ser202/Thr205, catalog MN1020 Thermo Fisher Scientific, 1:500). Subsequently, brain sections were washed with PBS buffer and incubated with secondary antibodies at the following dilutions: Goat anti-rabbit or anti-mouse secondary antibodies, conjugated with Alexa 488 or 594 (Life technologies), were used at 1:500. Finally, to identify the neurofibrillary tangles we used the Thioflavin-T dye as previously reported (Klunk et al., 2001). Briefly, sections were stained with 0.1% Thioflavin-T (Sigma-Aldrich) in 50% ethanol for 10 min as a final step and then mounted on glass slides and coverslip using an aqueous mounting medium.

2.12. Alkaline phosphatase activity

Alkaline phosphatase activity on brain slices was detected as previously described (Sebastian-Serrano et al., 2018b). Briefly, free-floating sections were washed twice with PBS, rinsed with Tris-HCl buffer (pH 7.5), and incubated with substrate BCIP/NBT (0.35 mM BCIP, 0.37 mM NBT, 5 mM $MgCl_2$, 100 mM Tris buffer, pH 9.5) in the presence or absence of 5 mM levamisole about 40 min until optimal staining intensity was obtained (Sigma-Aldrich, St. Louis, MO, United States). After washing with Tris-HCl buffer, sections were mounted on glass slides with an anti-fading solution. Background signal was determined pre-incubating brain slices with 5 mM levamisole 40 min before adding the BCIP/NBT substrate in presence of levamisole. To quantify the enzymatic reaction, we measured the amount of BCIP/NBT precipitates deposited on the hippocampus of all groups of mice. Values correspond to the mean intensity value of the pixel in eight-byte images containing the hippocampus subtracting the corresponding background signal (scale 0–255 with 0 = white and 255 = black).

For the analysis of TNAP activity in WT and TNAP OE mice transduced with pLOX-CW-CRE lentivirus, we represented the fold increase of the covered area by the staining in the injected (ipsilateral) dentate gyrus versus the contralateral dentate gyrus. The area fraction calculation was obtained using microscope images processed with the Colour deconvolution plugin (Image J) under a fixed intensity threshold (around 7.5% of the saturated pixels).

Human brain samples were homogenates with a Teflon glass homogenizer in 10 mm Tris-HCl buffer, pH 8.0, supplemented with 0.25 M sucrose and protease inhibitor mixture (EDTA-free CompleteTM, Roche Diagnostics) or with a protease inhibitor mixture containing 1 mm PMSF, 10 μg/mL aprotinin, 10 μg/mL leupeptin, and 50 μg/mL pepstatin. Aliquots from homogenates were assayed at 25 °C in the following reaction mix: 0.2 M diethanolamine buffer (Sigma-Aldrich), pH 9.8, 1 mM MgCl, and 5 mM *p*-nitrophenyl phosphate in the presence or in the absence of 5 mM levamisole. Reactions were stopped after 20 min with 0.1 M NaOH. Protein concentrations were quantified with the Bradford assay. TNAP activity was determined from the absorbance of the liberated *p*-nitrophenol at 405 nm and normalized to cellular protein content.

2.13. Image acquisition

Transmitted light images were acquired using a microscope (DM 1000, Leica) with a DFC450 CCD camera (Leica Microsystems GmbH) using Leica Application Suite (v4.1). Sections were photographed with Plan 4× dry objective lens (NA = 0.1) and insets with Plan S-Fluor 20× or 40× dry objective lens (NA = 0.90, Nikon) at room temperature.

Confocal images were acquired at room temperature with a TCS SPE microscope from Leica Microsystems equipped with a Plan Fluor 10× dry objective lens NA = 0.30, 40× Apochromat NA = 1.15 oil objective lens and 63× Apochromat NA = 1.3 oil objective lens (Leica Microsystems GmbH) and four different lasers lines (405, 488, 565 and 647 nm). Pictures were acquired using the Leica software LAS AF v2.2.1 software (Leica Microsystems GmbH) and representative slices converted to TIFF files using Fiji Software (ImageJ 1.52p, National Institutes of Health, Bethesda, Maryland, USA).

2.14. RNA extraction and quantitative real-time PCR (qRT-PCR)

Total RNA was extracted from hippocampi from human or adult mouse brains using a Speedtools total RNA Extraction Kit (Biotools) and following the manufacturer's instructions. Briefly, animals were sacrificed by cervical dislocation and hippocampi were immediately dissected and frozen using dry ice to proceed with total RNA isolation. After digestion with TURBO DNase (Ambion), 1 μg of total RNA was reverse transcribed with 6 μg of random primers, 350 μM dNTPs and M-MLV reverse transcriptase (all from Invitrogen).

qRT-PCR reaction mixtures containing DNA Master SYBR Green I mix (Applied Biosystems) were incubated at 95 °C for 20 s followed by 40 PCR cycles (95 °C for 1 s and 60 °C for 20 s) in a StepOnePlus Real-Time PCR System (Applied Biosystems). The specific primers for human gene encoding TNAP, *ALPL* were Fw 5′-CCACGTCTTCACATTTGGTG-3′ and Rv 5′-AGACTGCGCCTGGTAGTTGT-3′ amplifying exons from 9 to 10 (CCDS 217.1, Ensembl), for mouse gene encoding TNAP, *Akp2* Fw 5′-TGCCCTGAAACTCCAAAAGC-3′ and Rv 5′- TGTAGCTGGCCCTTAAGGATTC-3′ amplifying exons from 2 to 3 (CCDS18821.1, Ensembl); for mouse gene encoding muscarinic receptor M1, *Chmr1* Fw 5′-TCCCAACCCATCATCACTTT-3′ and Rv 5′-CATGACTGTGACAGGGAGGTAG-3′; and for both the human gene encoding *GAPDH* or mouse gene encoding *Gapdh* Fw 5′-CACCACCAACTGCTTAGCCC-3′ and Rv 5′-TGTGGTCATGAGCCCTTCC-3′. Expression levels of mRNA were represented as $2^{-\Delta\Delta Ct}$, where average cycle threshold (Ct) was obtained from triplicates of each sample. First, ΔCt means were normalized to parallel amplification of GAPDH as endogenous control. Next, ΔΔCt means were normalized to the average of corresponding controls.

2.15. Collection of CSF samples

The CSF samples from all the genotypes were collected as described by de Diego-Garcia et al. (de Diego-Garcia et al., 2020) being the experimenter blinded to the genotype of mice. Briefly, mice were anesthetized with isoflurane diluted in 50% O_2 and placed in a stereotaxic frame with the head forming a nearly 135° angle with the body. Mice were kept under anaesthesia during the surgery. The CSF of the four mouse groups described above was collected from the cisterna magna with a pulled capillary. Skin and muscle were dissected away to expose the dura mater overlying the cisterna magna before withdrawing CSF with a pulled capillary. Blood vessels were carefully avoided when penetrating the dura mater with the capillary tube in order to prevent contamination by plasma proteins. CSF was immediately frozen on dry ice.

2.16. Dephosphorylation assays

Tau dephosphorylation was performed as previously described (Diaz-Hernandez et al., 2010). Briefly, hyperphosphorylated Tau, obtained from insect cell culture infected with baculovirus expressing Tau protein, was incubated with one enzyme unit of TNAP for 1 h at 37 °C in PBS buffer pH 9.8. After dephosphorylation, the mixture was boiled for 5 min to inactivate the enzyme.

2.17. Tissue processing for Western blot

Mouse samples. Extracts for Western blot analysis were prepared by homogenizing fresh dissected mouse hippocampal area in ice-cold extraction buffer containing 20 mM Hepes, 100 mM NaCl, 50 mM NaF, 5 mM EDTA, 5 mM Na_3VO_4 (all from Sigma-Aldrich), 1% Triton X-100, okadaic acid (Calbiochem), and Complete TM Protease Inhibitor Cocktail Tablets (Roche Diagnostics GmbH), pH 7.4. The samples were homogenized at 4 °C, and protein content was determined by Bradford assay.

Human samples. Fresh samples of the hippocampus were obtained at the time of the autopsy, and they were immediately frozen in dry ice and stored at −80 °C for biochemical studies. Control, AD and PiD brain samples were processed following the same protocol as described for mouse samples.

2.18. Sarkosyl extraction

Aggregated Tau was isolated following the protocol described by Greenberg and Davies (Greenberg and Davies, 1990). The tissue was homogenized in 3 volumes of buffer H (10 mM Tris, pH 7.4, 0.8 M NaCl, 1 mM EGTA, 10% sucrose, 1 mM phenylmethylsulfonyl fluoride, protease inhibitors). The homogenate was centrifuged for 20 min at 27,200 *g* and 4 °C. The supernatant was then mixed with 1% N-lauroylsarcosinate (Sarcosyl) and 1% mercaptoethanol, incubated for 1 h at 37 °C, and centrifuged for 35 min at 150,000 *g* at room temperature. The pellets were resuspended in 0.5 volumes of 10 mM Tris, 154 mM NaCl and used for immunoblot analysis.

2.18.1. Immunoblot analysis

Total protein extracts (20 μg) from the hippocampi of mice or human samples were electrophoresed on 10 or 12% SDS- PAGE gels and transferred to nitrocellulose membranes (Amersham Biosciences). The PBS-buffer containing 0.1% (*v*/v) Tween-20 (PBS-T) and 5% non-fat dried milk was used as a blocking medium for 1 h at room temperature. Incubation with antibodies was performed overnight at 4 °C. The membranes were washed for 10 min with PBS-T three times and incubated for 1 h at room temperature with secondary antibodies.

The following primary antibodies were used at the dilutions specified in parentheses: rabbit anti-TNAP (catalog GTX62596, GeneTex, 1:10,000;); mouse anti-Tau-1 (recognizes dephosphorylated Tau, catalog MAB342, Chemicon, 1:1000); mouse anti-Tau AT8 (phospho Tau, catalog MN1020 Thermo Fisher Scientific, 1:500); rabbit anti-cFos (catalog sc-7202, Santa Cruz Biotechnologies, 1:200); rabbit anti-M1R (catalog AB5164, Merck Millipore, 1:250); mouse anti-α-Tubulin (catalog T5168, Sigma-Aldrich, 1:10,000); rabbit anti-GAPDH (catalog G9545, Sigma-Aldrich, 1:40,000), or mouse anti-β actin (catalog A5441, Sigma-Aldrich, 1:10,000). Secondary antibodies, goat anti- rabbit or anti-mouse IgGs coupled to horse-radish peroxidase (HRP, Amersham GE Healthcare) used at 1:1000 or 1:5000, respectively were used. Protein bands were visualized by ECL Pro chemiluminescence (Amersham GE Healthcare). Protein expression was standardized by the expression of GAPDH, α-Tubulin or ß-actin from the same experiment. For CSF samples, total protein levels detected by Ponceau staining were used for normalization purpose (Collins et al., 2015).

Gel band images were captured with ImageQuant LAS 500 (GE Healthcare Life Sciences) and analysed using ImageJ software (v1.52n, NIH, Bethesda, MD, United States), without applying any background subtraction. In the figures, the representative Western blot images show only the bands measured.

2.18.2. Cell counting

For the counting of hippocampal Cleaved Caspase-3 or M1R-positive cells, parasagittal brain sections (6–10 slices per mouse and at least 4 mice per genotype) were employed. Cleaved Caspase-3 positive cells and M1R-positive cells were identified by immunohistochemistry techniques, counting the number of them present in the whole hippocampus of each slice. The lateral ventricle area was determined by measuring the ventricle area in at least 4 serial parasagittal sections (harvested every 200 μm) per mouse in at least 5 mice per genotype. To quantify the number of hippocampal NeuN, AT8, or double AT8 / NeuN positive cells, the CA3 area of the hippocampus was identified by a double co-staining using DAPI dye (to delimit the granular layer) and calbindin (to mark the mossy fibers). Confocal images of CA3 were acquired from 4 different sagittal brain slices per mouse on at least 4 mice per condition. Two single focal planes per each section were acquired. The final value shows the percentage of neuronal density or AT8 neuronal density per area of the CA3 granular layer.

In the case of TNAP OE and WT mice transduced with lentivirus, we counted the hippocampal AT8 positive cells present in the surrounding area of the injection, covering it up to 200 μm away from the injection scar. We analysed at least 4–5 slices per mouse and from 5 mice per genotype.

2.19. Statistics

Data are shown as mean values ±95% CI. The numbers of mice per group or genotype used in each experiment are annotated as n in the corresponding figure legends. Figures and statistical analyses were generated using GraphPad Prism (version 6.00 for Windows, GraphPad Software, San Diego, CA, USA, www.graphpad.com). To assess whether the data met the normal distribution the Shapiro-Wilk or Kolmogorov-Smirnov tests were used. For two-group comparison, data were analysed with two-tailed unpaired Student's *t*-test, and for multiple comparisons with one-way ANOVA followed by Tukey's post hoc test. The statistical test used and *p*-values are indicated in each figure legend. Significance was considered at $^{*}P < 0.05$, $^{**}P < 0.01$, $^{***}P < 0.001$ or $^{****}P < 0.0001$ throughout the study.

2.19.1. Study approval

The protocol for animal experiments was approved by the Committee of Animal Experiments at the Universidad Complutense de Madrid and the Environmental Counseling of the Comunidad de Madrid, Spain (PROEX 374/15 and PROEX 185/17).

For human samples, a written informed consent for brain removal after death for diagnostic and research purposes was obtained from the brain donors and/or next of kin. Procedures, information and consent forms were approved by the Bioethics Subcommittee of Fundación Cien Madrid, Spain (S19001).

3. Results

3.1. Brains from patients with tauopathies manifest TNAP upregulation

To elucidate the cause of the high TNAP activity detected in the hippocampus of both sporadic and familial AD patients (Vardy et al., 2012), we first measured the levels of this protein in hippocampal samples from AD patients using a specific TNAP antibody (supplementary fig. 1A). These individuals presented 1.5 ± 0.2 fold more hippocampal TNAP protein expression than age-matched controls (Fig. 1A-B). In agreement with a previous report (Diaz-Hernandez et al., 2010), 81.8% of these AD patients also showed a significant increase in hippocampal *ALPL* mRNA levels (0.8 ± 0.2 fold more) compared with age-

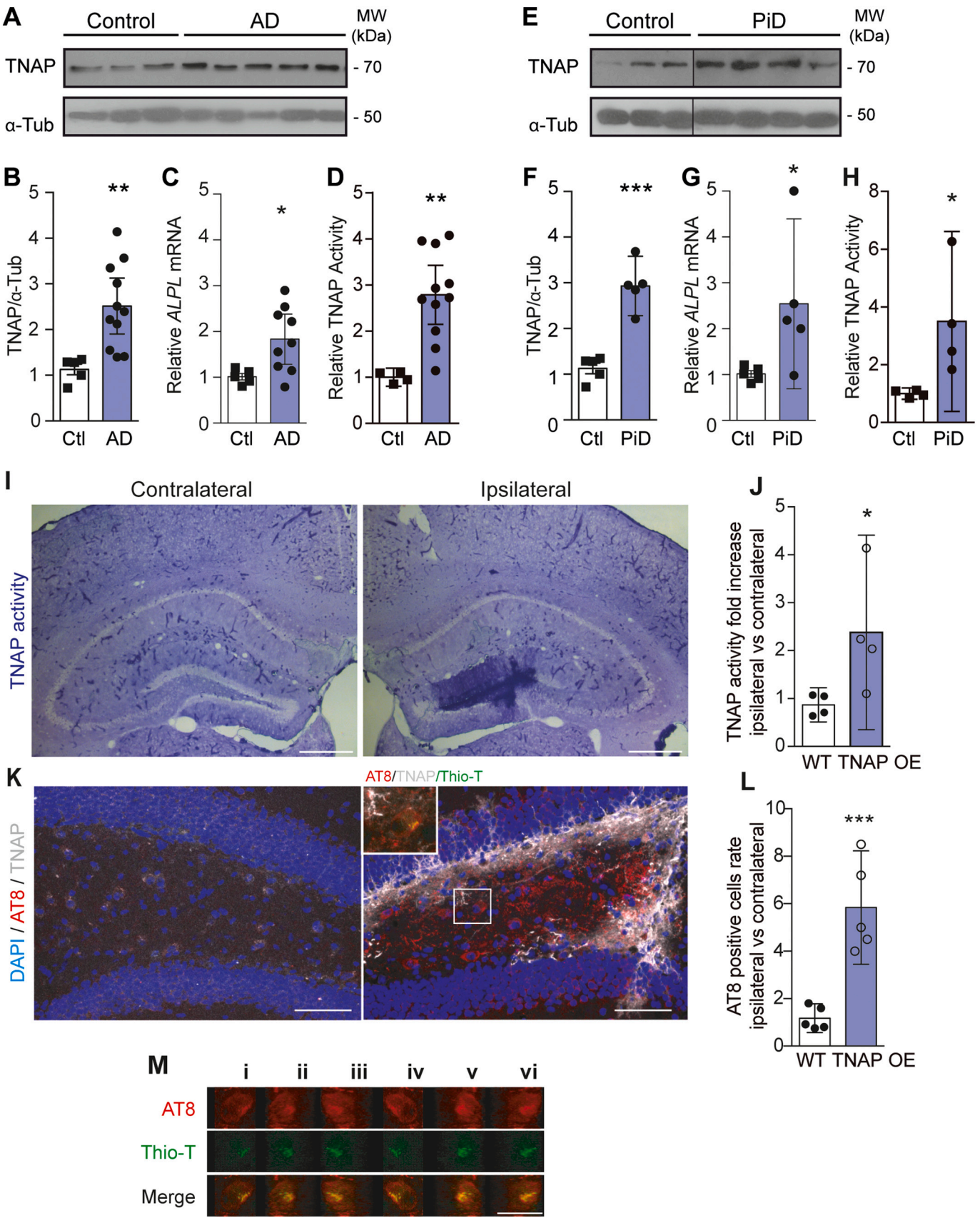

(caption on next page)

Fig. 1. Human tauopathy patients show a cerebral TNAP upregulation, being this condition sufficient to induce an hyperphosphorylation of intracellular Tau protein. (A-H) Representative immunoblot of TNAP using homogenates from hippocampal necropsies from (A) Alzheimer's disease (AD) or (E) Pick's disease (PiD) patients and their corresponding non-affected individuals (Ctl). Line indicates that lanes were run on the same gel but were non-contiguous. Quantification of TNAP protein levels in homogenates from hippocampal necropsies from (B) AD ($n = 11$) and (F) PiD patients and non-affected individuals ($n = 5$ each). Levels of α-tubulin (α-Tub) were used as loading control for normalization purposes. qRT-PCR analysis of *ALPL* mRNA from the hippocampus of (C) AD ($n = 9$) and (G) PiD (n = 5) patients and Ctl (n = 5). TNAP activity from hippocampal homogenates of (D) AD (n = 11) and (H) PiD ($n = 4$) patients and Ctl (n = 4).(I) Representative images of TNAP enzymatic assay on virus-injected brain sections from TNAP over-expressing (TNAP OE) mice show that Cre expression clearly increases TNAP activity in the ipsilateral hippocampus, not in the contralateral one. Scale bar = 0.2 mm. (J) The graph shows the TNAP activity ratio between ipsi- and contralateral sides from TNAP OE and WT mice intrahippocampal injected with Cre-expressing lentivirus ($n = 4$ mice per genotype). (K) Representative confocal immunofluorescence images of contralateral and ipsilateral hippocampal sides from TNAP OE mice stained with nuclear dye DAPI (blue), phospho-Tau Ser202/Thr205 (AT8, red), and TNAP (gray) antibodies 7 days after Cre-expressing lentivirus intrahippocampal injection (i.h). Insert corresponds to 2× magnification of the selected area. Green channel corresponds to Thioflavin-T (Thio-T) staining. Scale bar = 50 μm. (L) The graph shows the ratio of AT8-positive cells between ipsilateral- versus contralateral-sides in WT ($n = 5$) and TNAP OE mice (n = 5) 7 days after i.h. (M) Montage showing confocal images sequence of a hippocampal cell indicated in K. Image sequence (i to vi) correspond to rotated 60°images respect the previous one. Individual channels corresponding to AT8 (red) and Thioflavin-T (green) and merged are shown. Scale bar = 20 μm. Data are represented as means ±95% CI. $^{*}P < 0.05$, $^{**}P < 0.01$ or $^{***}P < 0.001$ using two tails unpaired Student's *t*-test. (For interpretation of the references to colour in this figure legend, the reader is referred to the web version of this article.)

matched controls (Fig. 1C). Similar increases in TNAP protein (1.9 ± 0.2 fold more) and its messenger (1.5 ± 0.6 fold more) were detected in hippocampal samples isolated from patients with PiD (Fig. 1E-G). Accordantly with the present results and those previously reported (Diaz-Hernandez et al., 2010), we found that AD and PiD patients present an increased brain TNAP activity in the brain than that detected in age-matched controls (2.8 ± 0.4 and 3.5. ± 2.9 fold more respectively, Fig. 1D and H).

3.2. TNAP overexpression promotes intracellular tau phosphorylation

To elucidate whether TNAP dysregulation is a pathological consequence or plays a triggering role in tauopathies, we analysed if an increase in TNAP expression and function might affect the levels of intracellular phosphorylated Tau. To address this question, we used $Hprt^{ALPL}$ mice harbouring a floxed "stop cassette" and the human *ALPL* cDNA inserted into the *Hprt* locus on the X chromosome. In these mice, Cre expression results in excision of the stop cassette and transgene expression leading to TNAP overexpression (TNAP OE). A Cre lentiviral

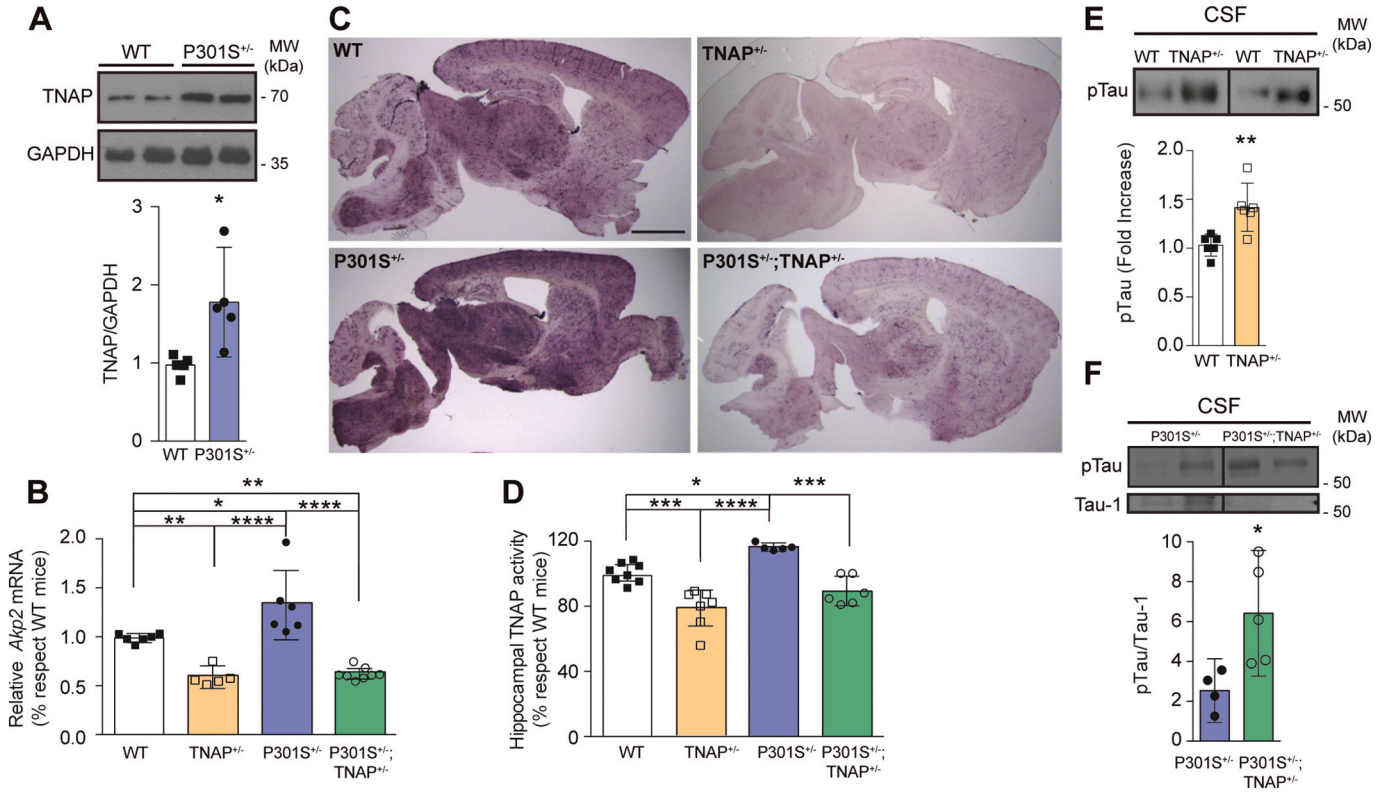

Fig. 2. TNAP haploinsufficiency in P301S mice normalize the levels of ecto-enzyme. (A) Representative immunoblot of TNAP and quantification of protein levels in homogenates from the hippocampi of 9-month-old $P301S^{+/-}$ and wild-type (WT) mice ($n = 5$ or 6 respectively) of the same age. α-tubulin (α-Tub) was used as loading control. (B) qRT-PCR analysis of *Akp2* mRNA in the hippocampi of WT ($n = 6$); $TNAP^{+/-}$ (n = 5); $P301S^{+/-}$ (n = 6) and double transgenic $P301S^{+/-}$;$TNAP^{+/-}$ mice ($n = 8$). (C) TNAP enzymatic assays on brain slices shows an overall decrease in $TNAP^{+/-}$ mice compared with WT animals, even in the P301S genetic background. Scale bar: 0.7 mm. (D) Graph shows quantification of the hippocampal TNAP activity ($n = 5$–8 mice per genotype). The 100% value corresponds to the amount of precipitated BCIP/NBT detected in the hippocampi of WT mice. (E) Representative immunoblot and quantification of phospho-Tau (Ser202/Thr205) protein levels in cerebrospinal fluid (CSF) samples from $TNAP^{+/-}$ mice and their corresponding WT littermates (n = 6 respectively). (F) Representative immunoblot and quantification of phospho-Tau (AT8) versus dephosphorylated Tau (Tau-1) ratio in CSF samples from $P301S^{+/-}$ and $P301S^{+/-}$;$TNAP^{+/-}$ mice ($n = 4$ and 5 respectively). Data are represented as means ±95% CI. $^{*}P < 0.05$, $^{**}P < 0.01$, $^{***}P < 0.001$ or $^{****}P < 0.0001$ using two tails unpaired Student's *t*-test or ANOVA followed by Tukey's post hoc test for multiple comparisons.

vector was injected into the hippocampus of adult TNAP OE and WT mice. Coronal sections containing ipsi- and contralateral hemispheres were analysed at 7 days after lentivirus injection. When we compare ipsi- against the contralateral side, alkaline phosphatase activity assay demonstrated that Cre expression clearly increased TNAP activity only in the ipsilateral hippocampus of TNAP OE mice, specifically in the surrounding area of the injection (Fig. 1I and Supplementary Fig. 1A). Indeed, dentate gyrus from ipsilateral side presented 1.5 ± 0.6-fold more TNAP activity than that from contralateral side (Fig. 1J). Afterwards, sections were stained with antibodies recognizing phosphorylated Tau at Ser202 and Thr205 (AT8) together with TNAP (Supplementary Fig. 2A) to elucidate whether TNAP overexpression affects the intracellular Tau protein phosphorylation rate. It is to note that TNAP OE mice showed 5.8 ± 0.8 fold increase in AT8 positive cells comparing ipsilateral versus contralateral hippocampus (Fig. 1K-L). Of note, a fifth of ipsilateral AT8-positive cells (21.0 ± 8.2%) presented intracellular inclusion bodies detected by Thioflavin-T staining (Fig. 1M and Supplementary Fig. 1B—C). However, intrahippocampal injection of CRE-expressing lentivirus did not induce an enrichment of AT8-positive cells nor an assembly of AT8/ThioT-positive intracellular aggregates in the ipsilateral hippocampus of WT mice (Supplementary Fig. 1A). Hence, all these results demonstrate that local rise in TNAP activity promotes phosphorylation of the intracellular Tau and its aggregation at specific regions independently of the injection injury.

3.3. The genetic reduction of TNAP improves cognitive and motor deficits in P301S mice and prolongs life expectancy

Once demonstrated that hippocampal TNAP upregulation observed in patients with tauopathies is sufficient to cause hyperphosphorylation and aggregation of intracellular Tau, we decided to study whether this condition is phenocopied by one of the most widely used mouse models of tauopathy, the P301S mice (Yoshiyama et al., 2007). The hippocampi of 9-month-old heterozygous P301S mice (P301S$^{+/-}$) showed 0.8 ± 0.2 fold more TNAP protein and 0.3 ± 0.1 fold more *Akp2* mRNA than their WT littermates (Fig. 2 A-B).

Since an increased TNAP activity has recently been linked to inflammatory processes (Bessueille et al., 2020; Graser et al., 2021), we wonder whether neuroinflammation associated with neurodegenerative diseases might be related with TNAP upregulation observed. To assess this hypothesis, we employed an LPS-induced neuroinflammation model. Additional groups of adult mice were treated intraperitoneally with LPS or the corresponding vehicle solution for 24 h. Immunoblotting approaches showed that LPS-treated mice exhibited a significant increase of hippocampal TNAP protein (147.9 ± 8.4% with respect to that detected in vehicle-treated mice, Supplementary Fig. 2B).

In a next step, to explore the potential value of a therapy based on preventing TNAP upregulation, we generated a new double transgenic mouse line by crossing P301S$^{+/-}$ and TNAP-deficient mice. Since homozygous TNAP null mice die before weaning (Narisawa et al., 1997), we crossed P301S$^{+/-}$ mice with heterozygous *Akp2*$^{+/-}$ animals (TNAP$^{+/-}$). The resulting mice had half of the *Akp2* genetic load (Fig. 2B), which led to reduced cerebral enzymatic activity (77.3 ± 4.5% of that detected in WT mice) (Fig. 2 C—D). As TNAP is an ectoenzyme able to dephosphorylate Tau at different sites in vitro (supplementary fig. 3A), we wondered whether a reduction in its activity would affect the eTau phosphorylation in vivo. Because phosphorylated intracellular Tau can be secreted and reach the CSF (Sebastian-Serrano et al., 2018a), we harvested CSF samples from the cisterna magna to analyse the phosphorylated eTau levels. Interestingly, this decrease in TNAP activity was sufficient to cause a significant signal accumulation corresponding to the AT8 antibody that identifies phosphorylated eTau in the CSF (42.0 ± 9.6% more than that detected in WT mice) (Fig. 2E). It is to note that we were unable to detect dephosphorylated eTau in TNAP$^{+/-}$ mice using the Tau-1 antibody (Supplementary Fig. 3B).

An initial analysis using TNAP enzymatic assays in parasagittal brain slices of the four groups of animals revealed that P301S$^{+/-}$ mice presented an overall increase (Fig. 2C). When focus on hippocampus, P301S$^{+/-}$ mice shown statistically significant higher TNAP activity than WT mice (114.6 ± 0.9% with respect to that detected in WT mice). However, this rise in activity was not present in P301S$^{+/-}$;TNAP$^{+/-}$ mice, which showed a non-statistically significant lower TNAP activity than WT mice (87.7 ± 3.5%, compared with WT mice, Fig. 2C-D). High magnification images of the hippocampus from the different analysed genotypes revealed that the increased TNAP activity in P301S mice is detected mainly in the parenchyma, independently of the activity observed in blood vessels (supplementary Fig. 2C). As expected, decreased TNAP activity in P301S$^{+/-}$;TNAP$^{+/-}$ mice induced a significant accumulation of phosphorylated eTau levels in the CSF (2.5-fold increase compared with P301S$^{+/-}$ mice, Fig. 2F).

To determine whether a deficient TNAP genetic load can delay or revert the onset of the phenotypic and behavioural alterations detected in P301S$^{+/-}$ mice, animals from the four genotypes were examined at two ages: 7 and 9 months. Data from behavioural tests showed that the onset of deficits began at 7 months only in P301S$^{+/-}$ mice (Fig. 3A-D). These deficits were manifested in an open field test, which revealed that P301S$^{+/-}$ mice explored the unprotected center area significantly more times than their WT control littermates. Since both groups travelled a similar total distance (Supplementary Fig. 3C) our results suggest that P301S$^{+/-}$ mice presented a decreased anxiety-like behaviour (Fig. 3A). To confirm this result, we performed the elevated-plus maze test, a specific test to analyse the anxiety-related behaviour. P301S$^{+/-}$ mice spent more time exploring the open arms, thus confirming a decreased anxiety-like behaviour (Fig. 3B). Interestingly, P301S$^{+/-}$;TNAP$^{+/-}$ mice did not show this behaviour, suggesting that reduced TNAP activity protects against the behavioural alterations developed by P301S$^{+/-}$ mice (Fig. 3A-B). Remarkably, when 9-month-old P301S$^{+/-}$;TNAP$^{+/-}$ mice were exposed again to the same maze than before, and although their behaviour might be affected by the previous experience acquired, they began to show a similar anxiety profile to that of P301S$^{+/-}$ animals at 7 months (Fig. 3A- B and Supplementary Fig. 3D-E). In addition, at 7 months of age, mice from the four genotypes did not show any motor deficiency detectable by a rotarod test or memory impairment detectable by the novel object recognition test (Fig. 3C-D). However, two months later, P301S$^{+/-}$ mice developed motor deficiency while P301S$^{+/-}$;TNAP$^{+/-}$ mice did not (Fig. 3C and Supplementary Fig. 3F). This observation therefore again suggests that reduced TNAP activity protects or delays the onset of behavioural symptoms in P301S$^{+/-}$ mice. At 9 months of age, P301S$^{+/-}$ mice also started to show a tendency to worsen memory capacity, showing lower learning capacity than three other groups of mice in the novel object recognition test (Fig. 3D and supplementary Fig. 3G). However, the P301S$^{+/-}$;TNAP$^{+/-}$ mice did not show this tendency (Fig. 3D and Supplementary Fig. 3G).

Given that the behavioural studies indicated that a reduced TNAP genetic load improved both early anxiety profile and later motor problems in P301S$^{+/-}$ mice, we explored whether this condition also improved the life expectancy of these animals. TNAP$^{+/-}$ mice presented a similar life expectancy to WT counterparts (a mean of 652.8 ± 41.8 days for WT mice, and 689.1 ± 44.4 days for TNAP$^{+/-}$ mice) (Fig. 3 E-F). In contrast, P301S$^{+/-}$ mice began to die as early as 270 days old, having a life expectancy of around 360 days. This scenario contrasted with P301S$^{+/-}$;TNAP$^{+/-}$ mice, almost 75% of which were still alive at 397 days (dotted line in Fig. 3F), when all P301S$^{+/-}$ were dead. Indeed, P301S$^{+/-}$;TNAP$^{+/-}$ animals showed a significantly higher life expectancy (472.3 ± 26.5 days) than their respective P301S$^{+/-}$ littermates (353.6 ± 6.6 days) (Fig. 3 E- F). These results confirmed a deleterious effect of increased TNAP activity on the development of tauopathies.

3.4. The genetic reduction of TNAP reduces neuronal death and deficiencies developed by P301S mice

In agreement with their shorter life expectancy and behavioural

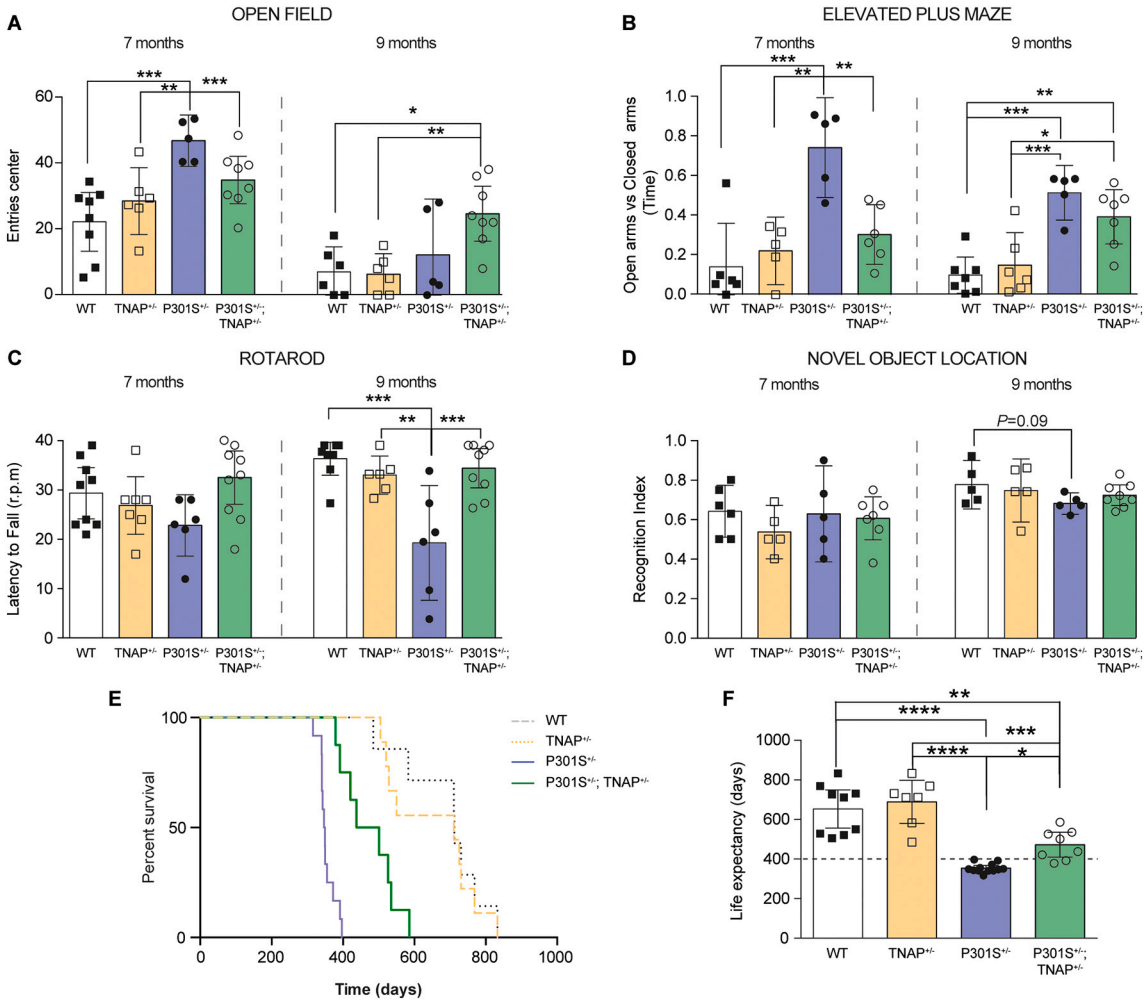

Fig. 3. TNAP haploinsufficiency improves behavioural, motor and memory endpoints in P301S mice. (A) Total number of center entries for WT, TNAP$^{+/-}$, P301S$^{+/-}$ and P301S$^{+/-}$;TNAP$^{+/-}$ mice at 7 and 9- month of age during the open field test. (B) Time in open versus closed arms for each of the above groups of mice in the elevated plus maze. (C) Graph shows the latency to fall for the four groups at 7 and 9 months of age. (D) Recognition index in the novel object recognition test for each of the above groups of mice. (E) Kaplan–Meier curves for cumulative survival show statistically significant differences between WT and P301S$^{+/-}$ ($P < 0.0001$) and P301S$^{+/-}$;TNAP$^{+/-}$ ($P < 0.01$) mice and between P301S$^{+/-}$ and P301S$^{+/-}$;TNAP$^{+/-}$ animals ($P < 0.05$). (F) Graphs shows the median survival of P301S$^{+/-}$ mice, 348 days, $n = 14$; WT, 711 days, n = 9; TNAP$^{+/-}$ 712 days, $n = 7$, and P301S$^{+/-}$;TNAP$^{+/-}$ 470 days, $n = 8$. WT vs P301S$^{+/-}$ $P < 0.0001$; WT vs P301S$^{+/-}$; TNAP$^{+/-}$ $P = 0.0012$; P301S$^{+/-}$ vs P301S$^{+/-}$;TNAP$^{+/-}$ $P = 0.031$ Data are represented as means ±95% CI. *$P < 0.05$, **$P < 0.01$, ***$P < 0.001$ or ****$P < 0.0001$ using ANOVA followed by Tukey's post hoc tests for multiple comparisons.

deficiencies, P301S$^{+/-}$ mice presented several pathological features (Yoshiyama et al., 2007), more precisely: i) cerebral atrophy detected by a significant increase in the lateral ventricle volume (Fig. 2C and Fig. 4D), ii) hippocampal neuronal loss that correlates with a higher number of histologically positive Cleaved Caspase-3 apoptotic cells (Fig. 4A and C), and iii) increased neuronal activity, which was measured analysing hippocampal levels of a classical molecular marker c-Fos protein by Western blot (Fig. 4E- F). However, P301S$^{+/-}$;TNAP$^{+/-}$ mice showed neither a significant cellular death rate, nor cerebral atrophy, nor increased neuronal activity (Fig. 4A-F). Supporting the neuroprotective effect induced by a decreased TNAP activity, P301S$^{+/-}$; TNAP$^{+/-}$ mice presented more CA3 hippocampal neurons identified by NeuN staining than P301S$^{+/-}$ animals (Fig. 4A- B). Interestingly, although P301S$^{+/-}$;TNAP$^{+/-}$ mice showed a higher percentage of phosphorylated intracellular aggregated Tau than the P301S$^{+/-}$ mice, nonetheless, both genotypes showed a similar density of hippocampal AT8-positive neurons (Fig. 5, A-B, Supplementary Fig. 4). Finally, it is to note that P301S$^{+/-}$;TNAP$^{+/-}$ mice that showed improved behaviour also presented a neuronal density similar to that observed in WT or TNAP$^{+/-}$ mice (Supplementary Fig. 5).

In previous work, it was demonstrated that the aberrant activation of muscarinic receptors M1 (M1R) by TNAP-dephosphorylated eTau induces neurotoxicity (Gomez-Ramos et al., 2006; Gomez-Ramos et al., 2008). Therefore, we decided to study whether the reduced TNAP genetic load affects M1R expression in the pathology. Immunoblot analysis of M1R in hippocampal lysates from the four groups reveal that P301S$^{+/-}$ mice showed a lower M1R expression levels than WT and TNAP$^{+/-}$ mice (Fig. 5C-D). Because this lowering was not related with transcriptional defects (Fig. 5E), a link with the cellular loss detected may be suggested. In support of this hypothesis, P301S$^{+/-}$;TNAP$^{+/-}$ mice, showing a lower neuronal loss than P301S$^{+/-}$ mice, presented similar M1R expression levels than WT and a higher number of M1 expressing neurons than P301S$^{+/-}$ mice (Fig. 5C-G).

3.5. *Pharmacological inhibition of TNAP reduces neurotoxicity and deficiencies developed by P301S mice in vivo*

Once the beneficial effects of TNAP haploinsufficiency on the tauopathy mouse model had been demonstrated, we tested whether in vivo pharmacological inhibition of this enzyme reproduced these

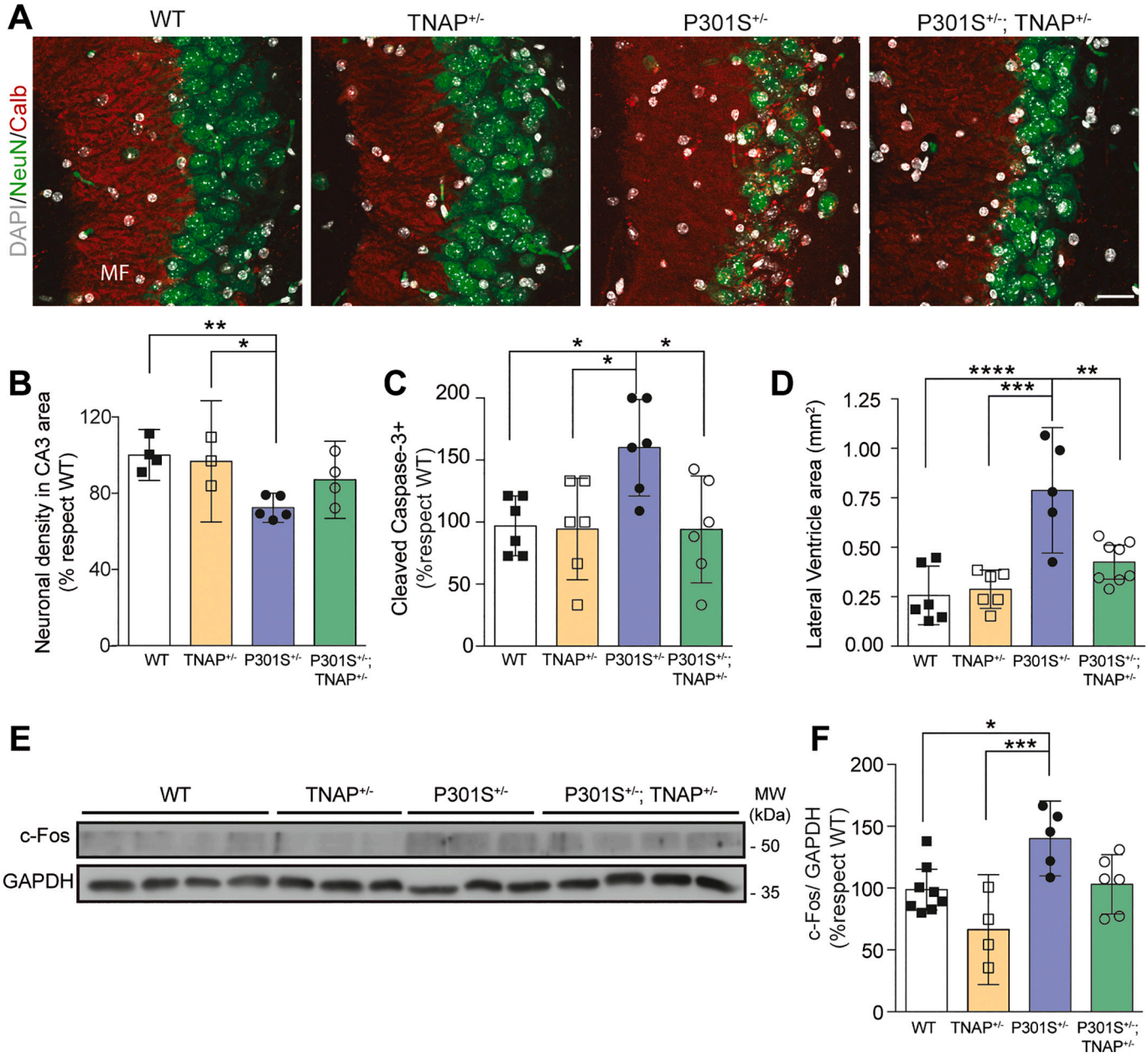

Fig. 4. A genetic loading reduction of TNAP prevents extracellular Tau-induced neurotoxicity. 9-month-old P301S$^{+/-}$ mice but not age-matched P301S$^{+/-}$; TNAP$^{+/-}$ animals presented marked neuronal death (A-C) and cerebral atrophy (D) compared with age-matched WT mice. (A) Parasagittal sections of hippocampus from four genotypes stained with specific neuronal marker (NeuN, green) and calbindin (Calb, red) antibodies to localize CA3 region. Scale bar: 20 μm. Graphs show quantification of positive NeuN (B), Cleaved Caspase-3 (C) cells in the hippocampus and lateral ventricle area (D) in WT (n = 4 or 6), TNAP$^{+/-}$ (*n* = 3 or 6), P301S$^{+/-}$ (n = 5 or 6), and P301S$^{+/-}$;TNAP$^{+/-}$ (n = 4 to 8) mice. The 100% value corresponds to the apoptotic cells (C) or lateral ventricle area (D) detected in WT mice. (*E*-F) Representative immunoblot and quantification of c-Fos protein levels for WT (n = 8), TNAP$^{+/-}$ (n = 4), P301S$^{+/-}$ (n = 5), and P301S$^{+/-}$;TNAP$^{+/-}$ (n = 7) mice at 9–10 month of age. Levels of GAPDH were used as loading control for normalization purposes when required. Results are mean ± 95% CI. *$P < 0.05$, **$P < 0.01$, ***$P < 0.001$ or ****$P < 0.0001$ using ANOVA followed by followed by Tukey's post hoc tests for multiple comparisons. MF = mossy fibbers. (For interpretation of the references to colour in this figure legend, the reader is referred to the web version of this article.)

improvements. To this end, a new set of P301S$^{+/-}$ and WT mice were treated daily with levamisole (9.3 mg/kg, intraperitoneally) or vehicle solution for 2 weeks. After treatment, mice were sacrificed and analysed. The capacity of levamisole to block brain TNAP was determined by measuring cerebral TNAP activity. A significant reduction of enzymatic activity was detected in levamisole-treated mice compared with vehicle-treated counterparts (levamisole-treated WT mice showed 73.3 ± 10.1% of TNAP activity detected in vehicle-treated WT mice whereas levamisole-treated P301S$^{+/-}$ mice showed 81.6 ± 6.5% of TNAP activity observed in vehicle-treated P301S$^{+/-}$ mice) (Fig. 6A-B and Supplementary Fig. 6A-B). Concordantly, immunoblot assays reveal a significant accumulation of phosphorylated eTau in CSF samples obtained from levamisole-treated P301S$^{+/-}$ mice (1.2 ± 0.1-fold increase in levamisole- treated mice than in vehicle-treated mice, Fig. 6C). Similarly, an acute i.c.v. administration of SBI-425, a non-permeable blood brain barrier selective TNAP antagonist, also induced a significant accumulation of phosphorylated eTau in CSF of WT mice (Supplementary Fig. 7). Interestingly, levamisole treatment reverted the cellular death and reduced the hippocampal neuronal loss but not ameliorated the ventricular atrophy in P301S+/− mice (Fig. 6D-F). It is

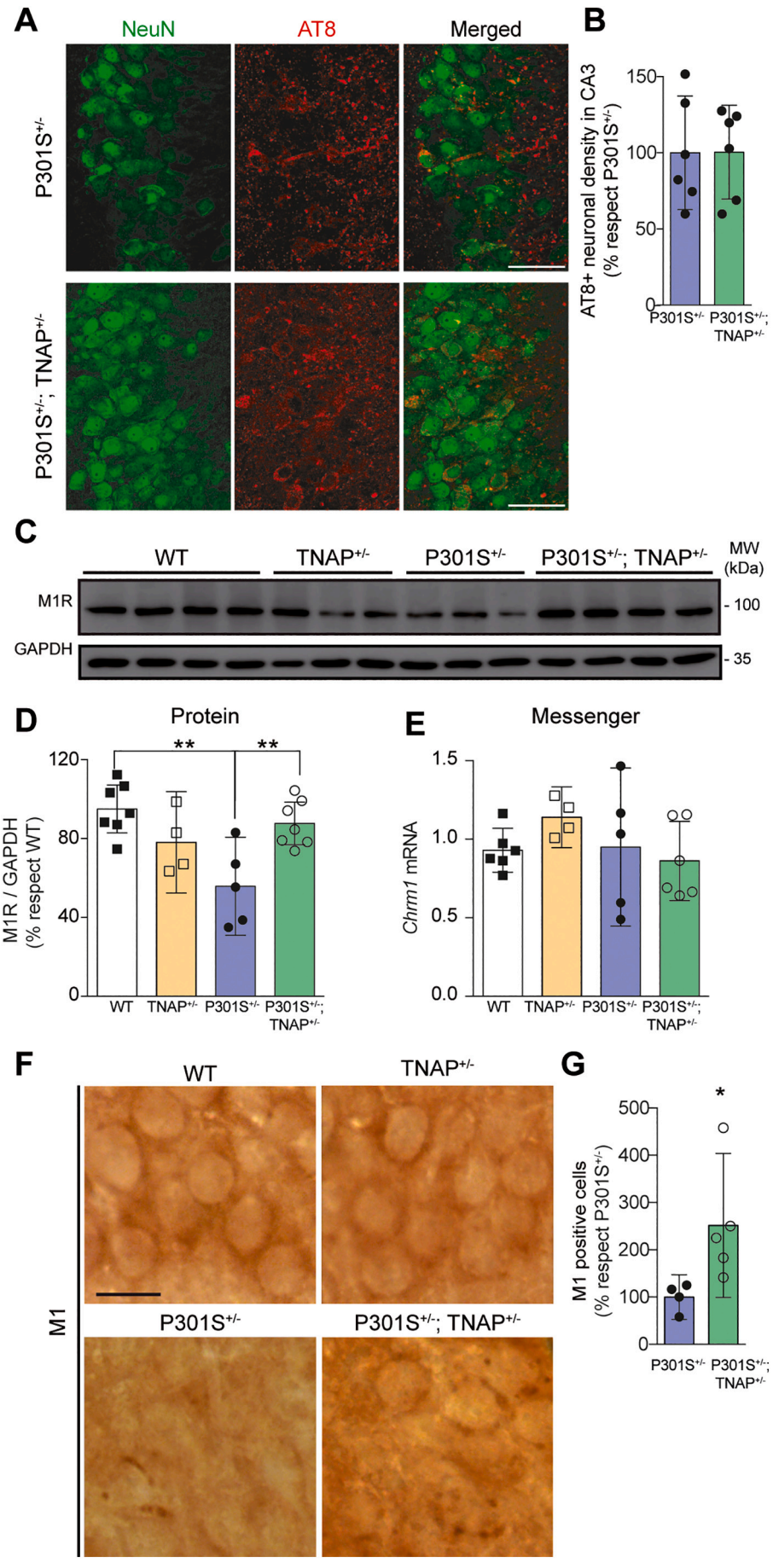

Fig. 5. TNAP haploinsuffiency reduces P301S-associated M1R loss. (A) Representative confocal immunofluorescence images of hippocampal (CA3) area of P301S$^{+/-}$ and P301S$^{+/-}$;TNAP+/− mice stained with AT8 (red channel) and NeuN (green channel) antibodies. Merged images of both channels are also showed. Scale bar = 50 μm. (B) The graph shows AT8-positive neuronal density (percentage of AT8-positive cells with respect to the total number of NeuN-positive cells) in CA3 area of P301S$^{+/-}$ and P301S$^{+/-}$;TNAP$^{+/-}$ mice (n = 6 per genotype). (C) Representative immunoblot and (D) quantification of M1R in hippocampal homogenates for each of the four groups of mice (n = 4–8 per group). Levels of GAPDH were used as loading control for normalization purposes when required. (E) qRT-PCR analysis of *Chrm1* (Cholinergic receptor muscarinic 1) mRNA from the hippocampi of WT (n = 6), TNAP$^{+/-}$ (n = 4), P301S$^{+/-}$ (n = 5) and double transgenic P301S$^{+/-}$;TNAP$^{+/-}$ mice (n = 6). (F) Representative images of immunohistochemical staining of the hippocampus of the four groups for M1R antibodies (scale bar = 20 μm). (G) Quantification of CA3 hippocampal M1-positive cells (P301S$^{+/-}$ n = 4; P301S$^{+/-}$;TNAP$^{+/-}$ n = 5). Results are mean ± 95% CI. *$P < 0.05$ or **$P < 0.01$ using two tails unpaired Student's t-test or ANOVA followed by Tukey's post hoc test for multiple comparisons. (For interpretation of the references to colour in this figure legend, the reader is referred to the web version of this article.)

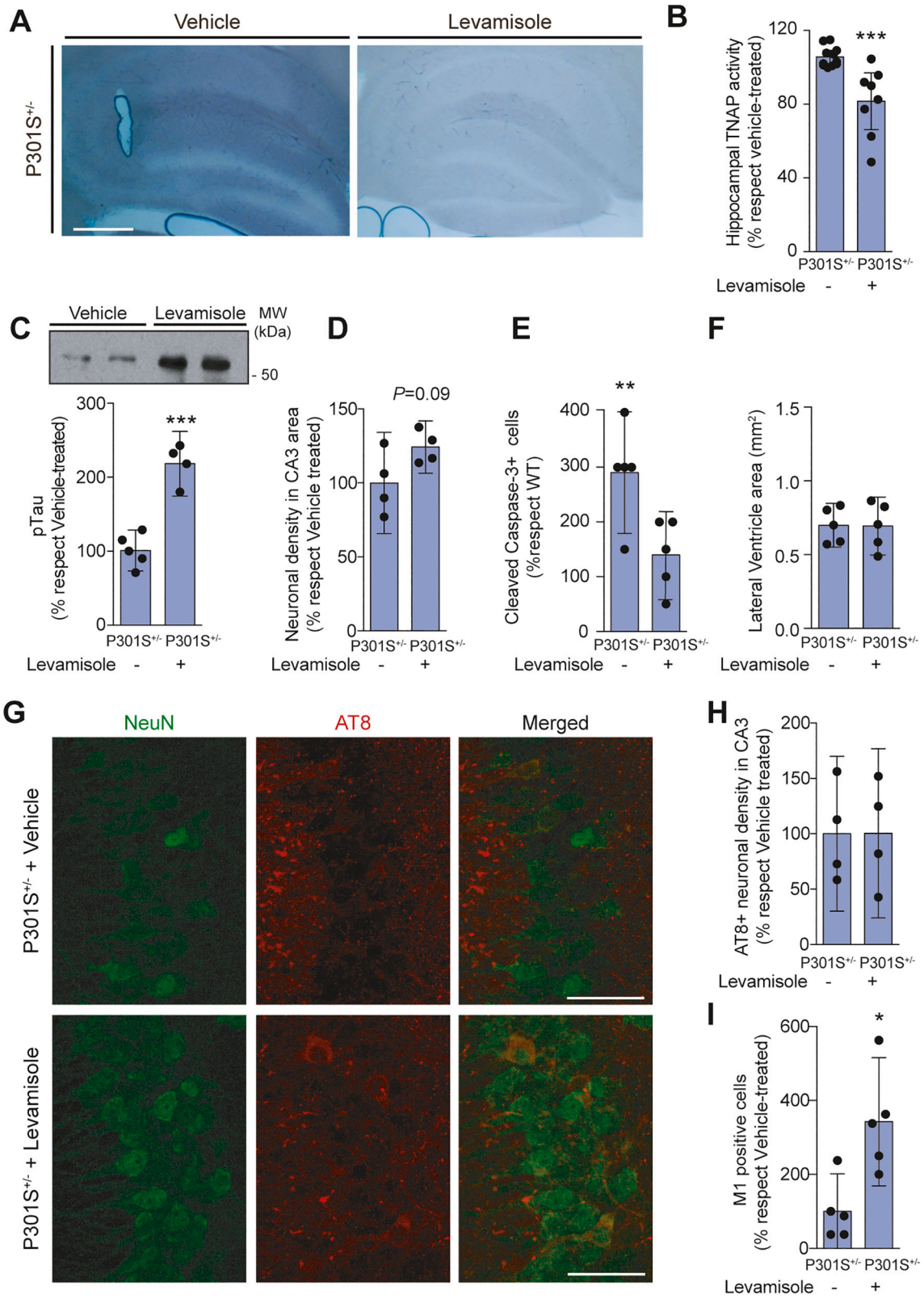

(caption on next page)

to note that levamisole-treatment did not induce any evident neurotoxic effect in the hippocampus of WT mice (Supplementary Fig. 6C-E). Similar to what was observed in P301S$^{+/-}$;TNAP$^{+/-}$ mice, TNAP inhibition did not modify the hippocampal AT8-positive neurons density in P301S$^{+/-}$ mice (Fig. 6G-H). Finally, a significant increase in M1R-expressing cells was detected in levamisole-treated compared with vehicle-treated P301S$^{+/-}$ mice (Fig. 6I). Altogether, these results suggest that TNAP pharmacological inhibition mimics some of the

Fig. 6. TNAP pharmacological inhibition reduces Tau-induced neurotoxicity by decreasing the eTau dephosphorylation. (A) TNAP enzymatic assay on brain slices shows an overall decrease in alkaline phosphatase activity in P301S$^{+/-}$ hippocampus when treated with levamisole. Scale bar: 0.2 mm. (B) Graph shows quantification of hippocampal TNAP activity (n = 10 or 6 mice per and condition). The 100% value corresponds to the amount of precipitated BCIP/NBT detected in the hippocampi of P301S$^{+/-}$ vehicle-treated mice. (C) Representative immunoblot analyses for phospho-Tau (Ser202/Thr205) identified with AT8 antibody in cerebrospinal fluid (CSF) obtained from P301S$^{+/-}$ mice treated with levamisole (n = 4) or with vehicle solution (n = 5), and graph corresponds to densitometric analysis. 9-month-old levamisole-treated P301S$^{+/-}$ mice showed higher number of CA3 hippocampal neurons (n = 4 per genotype and treatment) (D) lower cellular death (E) but similar cerebral atrophy (F) than P301S$^{+/-}$ animals treated with vehicle (n = 5 per genotype and treatment). (G) Representative confocal immunofluorescence images of hippocampal (CA3) area of P301S$^{+/-}$ mice treated with Levamisole or vehicle solution and stained with AT8 (red channel) and NeuN (green channel) antibodies (scale bar = 50 μm). Merged images containing both channels are also showed. (H) The graph shows AT8-positive neuronal density (percentage of AT8-positive cells with respect to the total number of NeuN-positive cells) in CA3 area of P301S$^{+/-}$ treated with levamisole or vehicle solution (n = 4 per condition). (I) Quantification of M1-positive cells (n = 5). Data are shown as means ±95% CI. *$P < 0.05$, **$P < 0.01$ or ***$P < 0.001$ using two tails unpaired Student's t-test. (For interpretation of the references to colour in this figure legend, the reader is referred to the web version of this article.)

improvements associated with TNAP haploinsuffiency in P301S mice.

4. Discussion

To our knowledge, this is the first study to address possible alterations in TNAP protein levels in human neurodegenerative pathologies, particularly in AD and PiD. Here, besides confirming that AD patients present high levels of brain TNAP as previously reported (Diaz-Hernandez et al., 2010; Vardy et al., 2012) we also found upregulated expression of TNAP in the brains of PiD's patients. Thereby, we postulate that this dysregulation could be a common feature of many tauopathies. Accordingly, the brains of P301S mice showed elevated TNAP protein levels associated with an increase in cerebral ectoenzyme activity. Given that TNAP mRNA levels are also augmented in human and mouse tauopathies, transcriptional mechanisms emerge as upregulation-causing factors, although we cannot exclude a post-transcriptional contribution. It is to note that local TNAP overexpression promotes aberrant hyperphosphorylation of intracellular Tau in neighbouring cells. Since TNAP is an ectoenzyme, an additional extracellular player involved in intracellular Tau phosphorylation is suggested. Previous studies demonstrated that TNAP-dephosphorylated eTau, conferring it greater neurotoxicity via aberrant muscarinic receptors activation (Diaz-Hernandez et al., 2010; Gomez-Ramos et al., 2009; Gomez-Ramos et al., 2008). Concordantly, in the present study we found that genetic disruption or pharmacological blockade of TNAP enriches the CSF of phosphorylated eTau at specific residues and reduces the loading of its dephosphorylated form. In agreement, in this work we also found that TNAP haploinsufficiency in P301S mice prevents neuronal hyperactivity, brain atrophy, and hippocampal neuronal death. Similar results were observed by the in vivo TNAP pharmacological blockade. This neuroprotective effect was accompanied by an improvement of behavioural responses of the double mutant P301S;TNAP mice. Furthermore, TNAP deficiency led to a significant increase in the lifespan of P301S mice. All these features point to TNAP inhibition as a new promising therapeutic strategy for tauopathies.

The stereotypical progression of Tau pathology between anatomically connected areas (Braak and Braak, 1991; Braak and Del Tredici, 2011) strongly suggests that synaptic components participate in the spread of the disease (Sebastian-Serrano et al., 2018a). The results of various approaches to track the propagation of Tau pathology, such as the intracranial injection of different Tau species (Clavaguera et al., 2009) or use of a transgenic mouse with restricted expression of human Tau in the entorhinal cortex (de Calignon et al., 2012; Liu et al., 2012), support this idea. All these works affirm that eTau is a major player in the spread and neurotoxicity associated with tauopathies. However, they neither elucidate if all eTau species have a similar spreading capacity or toxicity nor whether post-translational modifications may affect these capacities. Consequently, approaches reducing the total eTau levels emerge as potential therapeutic strategies. Our findings indicate that extracellular TNAP, which is mainly found at presynaptic levels in the CNS (Fonta et al., 2004; Sebastian-Serrano et al., 2016), favors eTau-induced neurotoxicity by promoting its dephosphorylation at specific sites. In this regard, the neuroprotective effects of TNAP ablation or inhibition might be explained by dephosphorylated eTau exerting a prion-like mechanism (Clavaguera et al., 2009; Holmes et al., 2013; Michel et al., 2014). However, the rescue of M1R-expressing neurons by TNAP ablation or pharmacological inhibition in P301S mice supports the notion that other non-prion-related mechanisms are involved. In this regard, we found that increased TNAP activity in P301S mice promotes the dephosphorylation of eTau specially those Ser and Thr residues recognized by AT8 and PHF1 antibodies, which has been described to trigger neuronal hyperactivity through M1R activation (Gomez-Ramos et al., 2006; Gomez-Ramos et al., 2009; Gomez-Ramos et al., 2008). In agreement, we detected increased levels of the immediate early gene c-Fos, a well-known molecular marker of neuronal activity (Morgan et al., 1987), in P301S but not in the double mutant mice. Given that neuronal activity causes endogenous Tau release (Pooler et al., 2013; Yamada et al., 2014), the dephosphorylation of this eTau by TNAP might in turn promote greater neuronal activity via M1R aberrant activation (Gomez-Ramos et al., 2008), closing in this way, a positive feedback loop that would contribute to worsening the pathology (Wu et al., 2016). In this line, previous in vitro studies demonstrated that TNAP-dephosphorylated eTau causes intracellular Tau phosphorylation (Gomez-Ramos et al., 2006) and an impairment of intracellular calcium homeostasis via aberrant muscarinic receptor activation, which finally leads to the death of hippocampal neurons expressing these receptors (Gomez-Ramos et al., 2009). In the same line, here, we find that in vivo TNAP overexpression causes the assembling of NFTs in neighbouring cells to those overexpressing the ectoenzyme. Thus, based on previous studies, it could be hypothesized that TNAP overexpression would promote dephosphorylation of the eTau basally released, which might cause the increase of intracellular phosphorylated Tau ratio in those nearby cells expressing muscarinic receptors. Contrarily, a reduction in cerebral TNAP activity prevented neuronal hyperactivity, loss of M1R-expressing cells and promoted hippocampal neuronal survival in P301S mice.

Our results not only demonstrate that cerebral TNAP upregulation is a common factor in AD and PiD, but that it may be also a triggering factor. However, the underlying molecular mechanisms inducing TNAP upregulation remain unknown. Interestingly, proinflammatory cytokines IL1β and TNFα enhance TNAP expression (Lencel et al., 2011). Since age-related neuroinflammation is associated with the onset of tauopathies (Sparkman and Johnson, 2008), TNAP upregulation caused by age-associated neuroinflammation might explain the late-onset of tauopathies. In this line, our results obtained with the LPS-induced neuroinflammation model strongly support this hypothesis. However, since neurodegeneration may also trigger a chronic neuroinflammatory reaction (Ransohoff, 2016), it would be as plausible to argue that neuroinflammation induced by Tau pathology leads to the increased TNAP observed in Tauopathies. Nevertheless, to clarify the causal relationship between both events and determinate which comes first, the chicken or the egg, additional studies should be done. But in addition to the neuroinflammation, other factors may be also contributing to TNAP upregulation observed in Tauopathies patients. So TNAP expression is also regulated by other factors such as the transcription factor Sp1, retinoic acid (Kiledjian and Kadesch, 1990; Orimo and Shimada, 2005), DNA

methylation (Delgado-Calle et al., 2011), and 1,35-dihydroxyvitamin D3 (Orimo and Shimada, 2006). On the other hand, TNAP promotes axonal growth and branching by regulating P2X receptors (Diez-Zaera et al., 2011; Sebastian-Serrano et al., 2016), so the increased TNAP expression detected in tauopathies might be a physiological response to counteract the pruning of synaptic contacts that occurs in these diseases (Sebastian-Serrano et al., 2018a; Yoshiyama et al., 2007). Nevertheless, this physiological response would also cause the eTau dephosphorylation collaterally, leading to a positive feedback loop that would aggravate the pathology. Therefore, it would be reasonable to expect the cerebral TNAP blockage strategy would have a positive beneficial/ risk ratio. Muchmore considering that the observed beneficial effects induced by the TNAP blockade might also be due to the impact that the blockade of this ectoenzyme causes on other factors related to Tau-induced neurotoxicity such as purinergic P2X receptors or the neuroinflammation (Di Lauro et al., 2022; Graser et al., 2021).

In recent years, new Tau-based therapies have attempted to tackle the toxic functions of Tau by lowering its extracellular levels. Specifically, immunotherapeutic approaches involving antibodies recognizing and removing eTau have given successful results in mouse models of tauopathy (Yanamandra et al., 2013). Nevertheless, passive immunization is not permanent, and it fails to increase the life expectancy of these strains of animals (d'Abramo et al., 2013; Wisniewski and Goni, 2015). Furthermore, active immunization via the administration of eTau might worsen the pathology and cause side effects like neuroinflammation (Rosenmann et al., 2006; Rozenstein-Tsalkovich et al., 2013). Therefore, additional therapeutic strategies should be considered (Kruger and Mandelkow, 2016). In this regard, the present results provide new integrative insight into the pathological mechanisms of Tau and uncover novel therapeutic avenues for treating AD and other tauopathies. Accordingly, we propose that the pharmacological inhibition of TNAP emerges as a suitable therapeutic strategy to avoid or slow down the neurotoxicity and disease progression induced by dephosphorylated eTau. In agreement, a recent study reports that Tau hyperphosphorylation in CSF occurs very early but decreases near the onset of cognitive decline (Barthelemy et al., 2020). Here we demonstrate that in vivo administration of two selective TNAP antagonists effectively promotes the eTau phosphorylation and reduces the neurotoxicity associated to tauopathies. However, given that the elevated dosage of levamisole required to reduce cerebral TNAP activity might trigger similar side effects to those observed when the drug is administered intracranially (Sebastian-Serrano et al., 2016), as well as other sides effects reported for this drug (Rehni and Singh, 2010), the development of new selective, potent and permeable blood-brain barrier TNAP inhibitors is needed. Furthermore, considering that TNAP is present in other parts of the body besides the brain, additional strategies should be valued to avoid possible side effects in these locations. One possibility might be to develop prodrugs releasing the active form of TNAP inhibitor after crossing the blood-brain barrier. Nevertheless, the absence of evident functional and behavioural deficits in the TNAP heterozygous mice, presenting reduced TNAP activity throughout the whole body (Sebastian-Serrano et al., 2018a) supports the safety of a therapeutic strategy based on TNAP inhibitors.

5. Conclusions

Here we demonstrated TNAP overexpression is a common hallmark of tauopathies and found that TNAP conditional overexpression causes aberrant Tau hyperphosphorylation in the neighbouring cells. In agreement with these findings, we found genetic disruption or pharmacological inhibition of TNAP prevented the pathological dephosphorylation of eTau and the associated neuronal loss. This neuroprotection correlates with a reduction of anxiety behaviours and motor deficiency and increasing memory capacity and life expectancy. Altogether, our result supports targeting TNAP as a novel strategy to avoid the pathological dephosphorylation of eTau and to counteract Tau pathogenesis and propagation.

Author contributions

A.S-S. generated and processed the transgenic mice, generated and analysed the samples, participated in experimental design, contributed to the interpretation of the data, and helped write the manuscript; J.M-R. contributed to the behavioural tests and processed samples; F.H. contributed to the processing the samples and the interpretation of the data, revised the manuscript and provided financial support for the work; C.dL and C.B. generated and analysed human samples; L.S. generated conditional transgenic mice samples; S·N generates the conditional TNAP transgenic mice; J.A and J.L.M. revised the manuscript and helped with the interpretation of data; M.D-H. participated in mouse generation and processing, generated and analysed the samples, designed the experimental approaches, contributed to the interpretation of the results, wrote the manuscript and provided financial support for the work. All authors read and approved the final manuscript.

Funding sources

This work was supported by funding from the following: Spanish Ministry of Economy and Competitiveness RTI2018-095753-B-I00 (to M.D.-H.), BFU2016-77885-P (to F.H.) and PGC2018-096177-B-I00 (to J. A.); European Union H2020 program H2020-MSCA-ITN-2017 number 766124 (to M.D-H); European Regional Development Funds from the Comunidad de Madrid S2017/BMD-3700 (NEUROMETAB-CM) (to F. H.); UCM-Santander Central Hispano Bank PR41/17–21,014 (to M.D-H); CIBERNED-ISCIII; and the Fundación R. Areces (to F.H.). A.S-S was hired by RTI2018-095753-B-I00 grant and as postdoctoral researcher by UCM (CT48/19), C.dL. and C.B. were hired by H2020-MSCA-ITN-2017 (grant number 766124), and J M-R had a fellowship from the Fundación La Caixa. This work was supported in part by ERDF.

Declaration of Competing Interest

The authors have declared that no conflict of interest exists.

Acknowledgements

Authors want to thank professors Gimenez-Cassina and Díaz-Nido for their generous gift of the lentiviral vector. We are grateful to all people working in the animal facility of the Faculty of Medicine (Universidad Complutense de Madrid, Spain), with a special mention to Soraya Martín-López for excellent technical assistance.

Appendix A. Supplementary data

Supplementary data to this article can be found online at https://doi.org/10.1016/j.nbd.2022.105632.

References

Ahmed, Z., et al., 2014. A novel in vivo model of tau propagation with rapid and progressive neurofibrillary tangle pathology: the pattern of spread is determined by connectivity, not proximity. Acta Neuropathol. 127, 667–683.
Barthelemy, N.R., et al., 2020. A soluble phosphorylated tau signature links tau, amyloid and the evolution of stages of dominantly inherited Alzheimer's disease. Nat. Med. 26, 398–407.
Bessueille, L., et al., 2020. Tissue-nonspecific alkaline phosphatase is an anti-inflammatory nucleotidase. Bone. 133, 115262.
Bondareff, W., et al., 1989. Neurofibrillary degeneration and neuronal loss in Alzheimer's disease. Neurobiol. Aging 10, 709–715.
Braak, H., Braak, E., 1991. Neuropathological stageing of Alzheimer-related changes. Acta Neuropathol. 82, 239–259.
Braak, H., Del Tredici, K., 2011. Alzheimer's pathogenesis: is there neuron-to-neuron propagation? Acta Neuropathol. 121, 589–595.
Chang, C.W., et al., 2021. Tau: enabler of diverse brain disorders and target of rapidly evolving therapeutic strategies. Science. 371.

Clavaguera, F., et al., 2009. Transmission and spreading of tauopathy in transgenic mouse brain. Nat. Cell Biol. 11, 909–913.
Collins, M.A., et al., 2015. Total protein is an effective loading control for cerebrospinal fluid western blots. J. Neurosci. Methods 251, 72–82.
d'Abramo, C., et al., 2013. Tau passive immunotherapy in mutant P301L mice: antibody affinity versus specificity. PLoS One 8, e62402.
de Calignon, A., et al., 2012. Propagation of tau pathology in a model of early Alzheimer's disease. Neuron. 73, 685–697.
de Diego-Garcia, L., et al., 2020. ATP measurement in cerebrospinal fluid using a microplate reader. Methods Mol. Biol. 2041, 233–241.
Delgado-Calle, J., et al., 2011. Epigenetic regulation of alkaline phosphatase in human cells of the osteoblastic lineage. Bone. 49, 830–838.
Di Lauro, C., et al., 2022. P2X7 receptor blockade reduces tau induced toxicity, therapeutic implications in tauopathies. Prog. Neurobiol. 208, 102173.
Diaz-Hernandez, M., et al., 2010. Tissue-nonspecific alkaline phosphatase promotes the neurotoxicity effect of extracellular tau. J. Biol. Chem. 285, 32539–32548.
Diez-Zaera, M., et al., 2011. Tissue-nonspecific alkaline phosphatase promotes axonal growth of hippocampal neurons. Mol. Biol. Cell 22, 1014–1024.
Fernandez, M., et al., 1998. Bioavailability of levamisole after intramuscular and oral administration in sheep. N. Z. Vet. J. 46, 173–176.
Fonta, C., et al., 2004. Areal and subcellular localization of the ubiquitous alkaline phosphatase in the primate cerebral cortex: evidence for a role in neurotransmission. Cereb. Cortex 14, 595–609.
Garcia, L.D., et al., 2018. The regulation of proteostasis in glial cells by nucleotide receptors is key in acute neuroinflammation. FASEB J. 32, 3020–3032.
Gomez-Ramos, A., et al., 2006. Extracellular tau is toxic to neuronal cells. FEBS Lett. 580, 4842–4850.
Gomez-Ramos, A., et al., 2008. Extracellular tau promotes intracellular calcium increase through M1 and M3 muscarinic receptors in neuronal cells. Mol. Cell. Neurosci. 37, 673–681.
Gomez-Ramos, A., et al., 2009. Characteristics and consequences of muscarinic receptor activation by tau protein. Eur. Neuropsychopharmacol. 19, 708–717.
Graser, S., et al., 2021. TNAP as a new player in chronic inflammatory conditions and metabolism. Int. J. Mol. Sci. 22.
Greenberg, S.G., Davies, P., 1990. A preparation of Alzheimer paired helical filaments that displays distinct tau proteins by polyacrylamide gel electrophoresis. Proc. Natl. Acad. Sci. U. S. A. 87, 5827–5831.
Holmes, B.B., et al., 2013. Heparan sulfate proteoglycans mediate internalization and propagation of specific proteopathic seeds. Proc. Natl. Acad. Sci. U. S. A. 110, E3138–E3147.
Hu, W., et al., 2016. Hyperphosphorylation determines both the spread and the morphology of tau pathology. Alzheimers Dement. 12, 1066–1077.
Kiledjian, M., Kadesch, T., 1990. Analysis of the human liver/bone/kidney alkaline phosphatase promoter in vivo and in vitro. Nucleic Acids Res. 18, 957–961.
Klunk, W.E., et al., 2001. Uncharged thioflavin-T derivatives bind to amyloid-beta protein with high affinity and readily enter the brain. Life Sci. 69, 1471–1484.
Kruger, L., Mandelkow, E.M., 2016. Tau neurotoxicity and rescue in animal models of human Tauopathies. Curr. Opin. Neurobiol. 36, 52–58.
Kurz, A., et al., 1998. Tau protein in cerebrospinal fluid is significantly increased at the earliest clinical stage of Alzheimer disease. Alzheimer Dis. Assoc. Disord. 12, 372–377.
Lee, V.M., et al., 2001. Neurodegenerative tauopathies. Annu. Rev. Neurosci. 24, 1121–1159.
Lencel, P., et al., 2011. Cell-specific effects of TNF-alpha and IL-1beta on alkaline phosphatase: implication for syndesmophyte formation and vascular calcification. Lab. Investig. 91, 1434–1442.
Levarska, L., et al., 2013. Of rodents and men: the mysterious interneuronal pilgrimage of misfolded protein tau in Alzheimer's disease. J. Alzheimers Dis. 37, 569–577.
Lim, F., et al., 2010. Reversibly immortalized human olfactory ensheathing glia from an elderly donor maintain neuroregenerative capacity. Glia. 58, 546–558.
Liu, L., et al., 2012. Trans-synaptic spread of tau pathology in vivo. PLoS One 7, e31302.
Michel, C.H., et al., 2014. Extracellular monomeric tau protein is sufficient to initiate the spread of tau protein pathology. J. Biol. Chem. 289, 956–967.
Morgan, J.I., et al., 1987. Mapping patterns of c-fos expression in the central nervous system after seizure. Science. 237, 192–197.
Narisawa, S., et al., 1997. Inactivation of two mouse alkaline phosphatase genes and establishment of a model of infantile hypophosphatasia. Dev. Dyn. 208, 432–446.
Orimo, H., Shimada, T., 2005. Regulation of the human tissue-nonspecific alkaline phosphatase gene expression by all-trans-retinoic acid in SaOS-2 osteosarcoma cell line. Bone. 36, 866–876.
Orimo, H., Shimada, T., 2006. Posttranscriptional modulation of the human tissue-nonspecific alkaline phosphatase gene expression by 1,25-dihydroxyvitamin D-3 in MG-63 osteoblastic osteosarcoma cells. Nutr. Res. 26, 227–234.
Peeraer, E., et al., 2015. Intracerebral injection of preformed synthetic tau fibrils initiates widespread tauopathy and neuronal loss in the brains of tau transgenic mice. Neurobiol. Dis. 73, 83–95.
Pooler, A.M., et al., 2013. Physiological release of endogenous tau is stimulated by neuronal activity. EMBO Rep. 14, 389–394.
Ransohoff, R.M., 2016. How neuroinflammation contributes to neurodegeneration. Science. 353, 777–783.
Rehni, A.K., Singh, T.G., 2010. Levamisole-induced reduction in seizure threshold: a possible role of nicotinic acetylcholine receptor-mediated pathway. Naunyn Schmiedeberg's Arch. Pharmacol. 382, 279–285.
Rosenmann, H., et al., 2006. Tauopathy-like abnormalities and neurologic deficits in mice immunized with neuronal tau protein. Arch. Neurol. 63, 1459–1467.
Rozenstein-Tsalkovich, L., et al., 2013. Repeated immunization of mice with phosphorylated-tau peptides causes neuroinflammation. Exp. Neurol. 248, 451–456.
Sebastian-Serrano, A., et al., 2016. Neurodevelopmental alterations and seizures developed by mouse model of infantile hypophosphatasia are associated with purinergic signalling deregulation. Hum. Mol. Genet. 25, 4143–4156.
Sebastian-Serrano, A., et al., 2018a. The neurotoxic role of extracellular tau protein. Int. J. Mol. Sci. 19.
Sebastian-Serrano, A., et al., 2018b. Haploinsufficient TNAP mice display decreased extracellular ATP levels and expression of Pannexin-1 channels. Front. Pharmacol. 9, 170.
Sheen, C.R., et al., 2015. Pathophysiological role of vascular smooth muscle alkaline phosphatase in medial artery calcification. J. Bone Miner. Res. 30, 824–836.
Sparkman, N.L., Johnson, R.W., 2008. Neuroinflammation associated with aging sensitizes the brain to the effects of infection or stress. Neuroimmunomodulation. 15, 323–330.
Vardy, E.R., et al., 2012. Alkaline phosphatase is increased in both brain and plasma in Alzheimer's disease. Neurodegener. Dis. 9, 31–37.
Wang, Y., Mandelkow, E., 2016. Tau in physiology and pathology. Nat. Rev. Neurosci. 17, 5–21.
Wisniewski, T., Goni, F., 2015. Immunotherapeutic approaches for Alzheimer's disease. Neuron. 85, 1162–1176.
Wu, J.W., et al., 2016. Neuronal activity enhances tau propagation and tau pathology in vivo. Nat. Neurosci. 19, 1085–1092.
Yamada, K., et al., 2014. Neuronal activity regulates extracellular tau in vivo. J. Exp. Med. 211, 387–393.
Yanamandra, K., et al., 2013. Anti-tau antibodies that block tau aggregate seeding in vitro markedly decrease pathology and improve cognition in vivo. Neuron. 80, 402–414.
Yoshiyama, Y., et al., 2007. Synapse loss and microglial activation precede tangles in a P301S tauopathy mouse model. Neuron. 53, 337–351.